Master's Thesis

Aerobic anoxygenic phototrophic bacteria and their photosynthetic membranes – imaging from macro- to nanoscale

Ole Franz

University of Jyväskylä

Department of Biological and Environmental Science

Nanoscience, Cell and Molecular Biology

19.10.2022

UNIVERSITY OF JYVÄSKYLÄ, Faculty of Mathematics and Science
Department of Biological and Environmental Science
Nanoscience, Cell and Molecular Biology

Ole Franz

Aerobic anoxygenic phototrophic bacteria and their photosynthetic membranes – imaging from macro- to nanoscale

MSc thesis: 56 p
Supervisors: Professor, Janne Ihalainen and Associate Professor, Jussi Toppari
Reviewers: Associate Professor, Lotta-Riina Sundberg and Associate Professor, Jussi Toppari

October 2022

Keywords: AFM, bacteriochlorophyll, endosphere, hyperspectral, light, photosynthesis, spectroscopy

While anaerobic anoxygenic phototrophic green or purple bacteria have been extensively researched, little is known about the ubiquity and function of aerobic anoxygenic phototrophic (AAP) bacteria in different environments. They perform photosynthesis in the presence of oxygen with the help of photosynthetic complexes including bacteriochlorophyll a. Equipped with this ability they have an advantage in oligotrophic environments. Previous research has focused on aquatic AAP bacteria, revealing new species, and developing hypotheses for their impact. Also, sometimes surprisingly high shares of procaryotic biomass comprised of AAP bacteria, for example in oligotrophic oceans, have been reported. However, functions and ubiquity of AAP bacteria in terrestrial environments have been neglected. Here, a self-built, low-cost imager for AAP bacteria detection is introduced. Based on UV-induced near-infrared fluorescence of bacteriochlorophyll a, it efficiently detected AAP bacteria colonies from environmental samples directly from Petri dishes. The method was compared with the commercially available option of using hyperspectral cameras for similar detection purposes. While the potential analysis depth of hyperspectral cameras proved to be larger, it was not possible to achieve a similarly specific and easy AAP bacteria identification with the here tested cameras and setups. Additionally, a method was developed to extract the photosynthetic membrane of *Sphingomonas glacialis* strain S2U11. Extracted material and whole cells were analyzed and compared spectroscopically, revealing that the extract contained intact photosynthetic complexes. Atomic force microscopy was used to image the isolated membranes and embedded protein complexes. The measured dimensions and packing of the photosynthetic structures fit well to the literature. However, the surrounding lipid bilayer measured only ~1 nm. The methods facilitate experiments with AAP bacteria previously reported only for anaerobic anoxygenic bacteria. They can help discovering differences between aerobic and anaerobic bacterial photosynthesis and species-specific novelties.

JYVÄSKYLÄN YLIOPISTO, Matemaattis-luonnontieteellinen tiedekunta
Bio- ja ympäristötieteiden laitos
Nanoscience, Solu- ja Molekyylibiologia

Ole Franz:	Aerobic anoxygenic phototrophic bacteria and their photosynthetic membranes – imaging from macro- to nanoscale
Pro gradu -tutkielma:	56 s
Työn ohjaajat:	Professori, Janne Ihalainen ja Apulaisprofessori, Jussi Toppari
Tarkastajat:	Apulaisprofessori, Lotta-Riina Sundberg ja Apulaisprofessori Jussi Toppari

Lokakuu 2022

TABLE OF CONTENTS

TERMS AND ABBREVIATIONS

TERMS

anoxygenic photosynthesis	photosynthesis in which oxygen is not produced as by-product
endosphere	space inside plants which can be colonized by bacteria
phyllosphere	surface of plants which is colonized by bacteria

ABBREVIATIONS

AAP	aerobic anoxygenic phototrophic
AFM	atomic force microscope/microscopy
BChl	bacteriochlorophyll
LH	light-harvesting
NIR	near-infrared
RC	reaction center
SNOM	scanning near-field optical microscopy

1 INTRODUCTION

Photosynthesis is a physiological process which transforms the sun light's energy into chemical energy. The most commonly known photosynthesis is carried out by plants, algae and cyanobacteria, which convert carbon dioxide to sugars and oxygen - vital requirements for animals on earth. However, there are also other forms of photosynthesis. Different groups of bacteria can perform photosynthesis for energy generation without producing oxygen. This has been long known for so-called purple bacteria, which grow in illuminated anaerobic environments, such as stagnant water bodies (Molisch 1907; Imhoff 2017). Oxygen suppresses the synthesis of bacteriochlorophylls (BChl), their primary photosynthetic pigments (Cohen-Bazire *et al.* 1957). Only about 40 years ago, aerobic anoxygenic phototrophic (AAP) bacteria were discovered which require oxygen for their photosynthetic metabolism (Shiba *et al.* 1979; Shiba and Simidu 1982). The late discovery is especially surprising as this diverse group of bacteria is nowadays estimated to account for a significant percentage of all microbial life in the oceans and other oligotrophic environments (Kolber *et al.* 2001; Schwalbach and Fuhrman 2005; Kolářová *et al.* 2019). For example, Lami and colleagues (2007) reported that 24% of all procaryotic life in their samples from the South Pacific Ocean were AAP bacteria. Other studies have reported that AAP bacteria abundance represented up to 28.5% of total procaryotic cells in the upper layer of freshwater lakes (Cepáková *et al.* 2016; Kolářová *et al.* 2019). However, terrestrial ubiquity of AAP bacteria has not been investigated as much.

It has been proposed that the initial production of oxygen by cyanobacteria during the Paleoproterozoic era created a selection pressure for previously anaerobic anoxygenic phototrophic bacteria to thrive in aerobic conditions (Beatty 2002; Yurkov and Hughes 2017). Another possibility is that originally heterotrophic, non-phototrophic bacteria gained the photosynthetic complex through horizontal gene transfer (Yurkov and Hughes 2017).

Heterotrophic AAP bacteria have a clear advantage over non-phototrophic organisms in extreme environments with few nutrients and consequently have been repeatedly isolated in such (George *et al.* 2020). While the ecological impact of this group of bacteria has not been fully understood, it is potentially playing significant roles in biogeochemical cycles such as the carbon cycle (Kolber *et al.* 2001; Koblížek *et al.* 2007; Boeuf *et al.* 2013)

AAP bacteria species diversity, biogeography and ubiquity, especially in terrestrial environments, is still poorly understood and requires further research (Galachyants et al. 2021). Therefore, efficient sampling and isolation methods are needed to discover more AAP species. Additionally, the detailed photosynthetic process and photosynthetic complex architecture in individual AAP species is still not well understood. According to Yurkov & Hughes (2017), the key differences between AAP bacteria and anaerobic purple non-sulfur bacteria regarding their photosynthetic electron transport chain and BChl a synthetic pathway are not clear yet, even though one relies on oxygen and the other only functions without it. Of course, the better mechanisms are understood, the better is the possibility to implement them in new applications. As of now, AAP bacteria have not been well studied for potential applications (George *et al.* 2020).

This work explores how different imaging techniques can help to shed more light on the diverse group of AAP bacteria and their individual photosynthetic complexes. Different macroscopic detection and characterization methods are briefly compared. The emphasis of this work is on the extraction of photosynthetic membranes from the *Sphingomonas glacialis* strain S2U11, originally isolated from plant endosphere and subsequent imaging with atomic force microscopy (AFM) in the nanoscale (Nissinen *et al.* 2012). This work presents a workflow for the membrane extraction from *S. glacialis* strain S2U11 and insights into the dimensions and architecture of the photosynthetic complex in its native membranes.

1.1 Aerobic anoxygenic photosynthesis

While most AAP bacteria have been isolated from aquatic environments, they have been also found in extreme terrestrial environments such as dust, organic soil crusts and the rhizosphere, endosphere and phyllosphere of plants (Fleischman and Kramer 1998; Kim et al. 2007; Csotonyi et al. 2010; Nissinen et al. 2012; Tang et al. 2021). However, the majority of AAP bacteria research has focused on the aquatic environment. The here studied strain was originally isolated from the endosphere of *Diapensia lapponica*. This extreme terrestrial environment can be challenging due to a mixture of temperature fluctuations, ultraviolet (UV) radiation and periodical drought stress, as well as severe nutrient limitations (Delmotte *et al.* 2009; Stiefel *et al.* 2013; Zervas *et al.* 2019). One way to cope with the oligotrophic environment can be to employ photosynthesis for energy production. This hypothesis was recently supported by Kopejtka and colleagues (2020) who found that the photosynthetic reaction center (RC) expression is suppressed by high glucose concentrations in AAP bacteria closely related to *S. glacialis*. Additionally, anoxygenic photosynthesis does not require water as electron donor which may be an important aspect for bacteria surviving in arid environments (Kolber *et al.* 2001). However, AAP bacteria are not close to being photoautotroph. According to Yurkov & Csotonyi (2009), 80% or more of the required cellular energy is provided by heterotrophy. The advantage of AAP is the increased carbon assimilatory efficiency, which describes the growth of microbial biomass per utilized amount of carbon. When exposed to light, AAP bacteria can yield double the amount of biomass compared to regular heterotrophs (Yurkov and Csotonyi 2009). This explains why AAP bacteria are thought to have a significant role in the marine carbon cycle (Yurkov and Csotonyi 2009).

The most studied phototrophic bacteria are the group of purple bacteria, which are anoxygenic species thriving in anaerobic conditions. In these bacteria, a variety of BChls and carotenoids are responsible for the absorption of light, while the electron transfer is mediated by the light-harvesting complexes LH1 and LH2, which are arranged around reaction centers (Ritz et al. 2002).

While AAP bacteria have similar components in their photosynthetic complexes, they are unable to utilize photosynthesis in anaerobic conditions. AAP bacteria are a phylogenetically diverse group, with species from different genera. They are united by possessing photosynthetic complexes consisting of type II reaction centers, LH1 complexes and BChl a. They are not independent of organic carbon, produce no oxygen and have relatively low levels of photosynthetic complexes compared to anaerobic anoxygenic phototrophic bacteria (Yurkov and Beatty 1998; Selyanin *et al.* 2015). Additionally, all AAP bacteria discovered so far contain a high abundance of carotenoids, lack Ribulose-1,5-biphosphate carboxylase/oxygenase (RuBisCO), which is used to fix CO_2, and are gram-negative (Yurkov and Beatty 1998; George et al. 2020). While anaerobic anoxygenic phototrophic bacteria have an extensive intracellular membrane system which accommodates the photosynthetic components, it has not been verified to what extend this system exists in various AAP bacteria (Yurkov and Beatty 1998). The precise location of photosynthetic complexes has not been discussed in recent studies about AAP bacteria.

While purple photosynthetic bacteria can have a large variety of BChl types, AAPs only possess BChl a. Interestingly, BChl a has been shown to accumulate in AAP bacteria only during dark periods after the cells have been exposed to light (Fleischman and Kramer 1998). Additionally, along with various carotenoids, rhodopsins have been identified as additional pigments, raising the question about their individual purpose (Kopejtka et al. 2020; R. Nissinen et al., unpublished). Carotenoids in photosynthetic systems can expand the usable wavelengths range by absorbing blue-green light and subsequent energy transfer to BChl (van Grondelle *et al.* 1994). They are also able to protect the cells from photooxidative damage during high intensity sun radiation, for example by quenching damaging singlet oxygen (Griffiths *et al.* 1955; Yurkov *et al.* 1993; Šlouf *et al.* 2012).

It has been reported, that both AAP and purple bacteria can contain light harvesting complexes 1 (LH1) and 2 (LH2) at different ratios. However, some AAP

species, such as the bacteria associated with *S. glacialis*, only contain LH1 complexes (Kopejtka et al. 2020; Nissinen et al., unpublished). The LH1 complex resembles a ring which consists of 16 heterodimer subunits. It harbors BChl a pigment molecules and can contain additional photosynthetic carotenoids (Yurkov and Beatty 1998; Qian et al. 2003; Tang et al. 2010). Previous studies have found that light intensity influences the amount of BChl a present in LH1-RC complexes of the AAP bacteria *Roseobacter litoralis*. The reported range reached from 39 ± 3 molecules in bright light to 115 ± 30 BChl a molecules in dark growing conditions per LH1-RC complex (Selyanin *et al.* 2015). This indicated that too much BChl pigments may be harmful for the bacteria in strong light, while it may benefit from increased light absorption in dark environments. Interestingly, the same study found that the number of reaction centers increased with light intensity from 480 RC units per cell in the dark to 1800 RC units per cell in the brightest conditions (Selyanin *et al.* 2015)

The recent characterization of strain AAP5, a close relative of *S. glacialis* and strain S2U11, also described its photosynthetic complex as a single ring of LH1 complexes around the central RC. According to electron microscopy images in the same study, the complex measured around 12 nm in diameter (Kopejtka *et al.* 2020).

1.2 *Sphingomonas* bacteria

The strain S2U11 used in this work belongs to the genus *Sphingomonas* which is a class of Alphaproteobacteria. It contains aerobic, gram-negative and non-spore-forming bacteria. It was first proposed by Yabuuchi and colleagues in 1990. Some members of this genus have been described early on as orange-pigmented, psychrotolerant bacteria, which were isolated from air, dust and environments in the Antarctic (Yabuuchi *et al.* 1990; Busse *et al.* 2003).

The *Sphingomonas glacialis* type strain was first isolated from alpine glacier dust (cryoconite) in 2011 and subsequently characterized by Zhang and colleagues

(Zhang *et al.* 2011). In the initial publication, the phototrophic characteristics were not mentioned. However, the recent characterization of the strain AAP5, which is closely related to *S. glacialis,* categorizes it as an AAP bacterium and presented spectra and DNA analysis indicating the presence of LH1 complexes, BChl a and xanthorhodopsin (Kopejtka *et al.* 2020, 2021)

Other *Sphingomonas* species, including *Sphingomonas natatorial*, *Sphingomonas ursincola, Sphingomonas kaistensis* and strain FukuSWIS1 have been found to be photoheterotrophic (Yabuuchi *et al.* 2002; Kim *et al.* 2007; Salka *et al.* 2014). Recently, *Sphingomonas* bacteria containing the *puf*M gene, which encodes the photosynthetic reaction center, were identified in the lake Baikal (Galachyants et al. 2021). Additionally, it has been reported that there is a high abundance of bacteria with aerobic anoxygenic phototrophic (AAP) genes in the phyllosphere, including *Sphingomonas* species (Atamna-Ismaeel *et al.* 2012). However, according to Kopejtka and colleagues (2020) only a fraction of discovered *Sphingomonas* species contain a photosynthesis gene cluster.

1.3 Imaging of phototrophic bacteria and photosynthetic membranes

BChl a has been known to fluoresce in the near-infrared wavelength range, which has been utilized since many years to identify bacteria containing BChl a with fluorescence microscopy or other spectroscopic methods (Pierson and Howard 1972; Kolber et al. 2001). The in-vivo absorption peak for BChl a incorporated in a LH1-RC complex is typically around 870 nm. The neighboring proteins are thought to influence the absorption so that peaks from 855 nm to 879 nm have been reported for different bacteria (Olsen *et al.* 1994; Yurkov and Hughes 2017). The previously mentioned characterization of a close relative of *S. glacialis* resulted in a measured absorption peak at 872 nm and a fluorescence peak at 886 nm in the near-infrared (NIR) region (Kopejtka *et al.* 2021).

Macroscopic bacteria colonies can be simply identified as phototrophic with appropriate excitation light and a NIR sensitive camera covered by a suitable filter which blocks all but NIR light. However, the previously published detection set-up employed a highly sensitive research camera which is not very accessible and cost effective (Zeng et al. 2014). In fact, CMOS and CCD sensors of all consumer-grade cameras are sensitive to infrared light but so-called hot mirrors are commonly installed in front of them to block the NIR and infrared light from reaching the sensor and disturbing the image. It is often possible to manually remove this hot mirror or use inexpensive night vision cameras, which use infrared light for illumination, to record NIR fluorescence. These cameras can be used together with a bandpass filter for non-NIR light to only allow the NIR fluorescence to reach the sensor. The excitation light can be in the blue or UV region where the so-called Soret bands of BChl absorb. Through internal conversion, BChl returns to the first electronic singlet state (S1). Transition to the ground state results in fluorescence emission in the NIR region (Lennarz and Lane 2013). Having the excitation wavelength far from the recorded fluorescence is useful for the detection, as there is a reduced risk of excitation light bleeding through the emission filter and affecting the measurement.

Generally, this low-cost approach enables more efficient and affordable screening. However, it is only possible to determine if bacteria colonies are positive or negative for BChl a. In order to further analyze the constituents of the photosynthetic complexes or distinguish between different AAP bacteria, more sophisticated spectroscopic methods are needed. The common approach is to use a fluorescence spectrometer to measure the absorbance and fluorescence peaks of suspended cells. Depending on the setup, it may be also possible to dry a swab of cells on a glass slide or measure the fluorescence directly from the Petri dish with the excitation light and sensor aimed at a well-isolated colony. This process may be tedious and time consuming depending on the number of samples.

Hyperspectral cameras combine the properties from imaging and spectroscopy by obtaining the spectrum for each pixel in a single recorded picture. They are therefore frequently used for different remote sensing methods to identify or analyze objects, processes, or species (Chang 2003). These cameras commonly function with a spectrograph placed behind the camera which contains a slit, collimating optics and a dispersive unit. This set-up splits single lines of the image into a dispersed spectra to cover the entire sensor. The intensity of each wavelength can then be read with a grayscale camera sensor (ElMasry and Sun 2010). These kinds of hyperspectral cameras are therefore line-scan cameras. Simultaneous bacterial colony identification on Petri dishes has been already demonstrated on various pathogens (Arrigoni *et al.* 2017). Hyperspectral cameras may be useful to detect AAP bacteria and possibly distinguish between colonies with different protein compositions or photosynthetic components. This analysis could be done for all colonies on a Petri dish at once, resulting in a significantly higher throughput compared to measuring individual spectra separately.

Hyperspectral cameras can be also attached to the camera ports of microscopes to analyze individual microbes. This has been used, for example, to differentiate between gram-positive and gram-negative bacteria cells (Park et al., 2015). NIR sensitive microscopy could enable the detection and possibly the isolation of AAP bacteria in diverse samples before culturing. This is relevant because it is still estimated that over 99% of environmental bacteria are currently not culturable (Lloyd *et al.* 2018). However, it is important to keep in mind that there are currently only few experimental options if single, unculturable cells are the only available material.

Analyzing AAP bacteria with imaging techniques can go beyond simple light microcopy. Atomic force microscopy (AFM) is a type of scanning probe microscopy which allows to image the topography of samples in sub-nanometer resolution (Binnig *et al.* 1986). The high resolution can easily resolve molecules and has been also used to study the native architecture and arrangements of

photosynthetic systems and complexes (Scheuring *et al.* 2007). The investigation of native photosynthetic membranes of different bacteria with AFM started in the 1990´s and has been extensively researched in the first decade of the 21th century (Worcester *et al.* 1990; Scheuring *et al.* 2004; Gonçalves *et al.* 2005; Scheuring and Sturgis 2009). Even though AFM can provide high-resolution structures and topographies, the method is unable to provide spectroscopic data.

Scanning near-field optical microscopy (SNOM) combines the resolution and topography recording characteristics of the AFM with localized, spectroscopic measurements in resolutions far beyond the diffraction limit. These measurements can include for example Fourier transform infrared spectroscopy (FTIR), fluorescence or Raman spectroscopy. SNOM imaging of the native photosynthetic complex could reveal new insights about the mechanisms of each contributing protein and their linkages.

The optimal way of studying a native membrane is in liquid, since it is the natural environment in which all structures remain hydrated and in functioning shape. This has been already successfully demonstrated when imaging supramolecular membrane assemblies with AFM (Bahatyrova *et al.* 2004; Scheuring and Sturgis 2009). However, also dehydrated membranes and embedded membrane proteins have been imaged with AFM and SNOM (Trudel *et al.* 2001; Berweger *et al.* 2013) While liquid imaging of biological material is possible and constantly improving, in-air imaging is still easier to perform with SNOM (O'Callahan *et al.* 2020). Only recently, liquid SNOM imaging of photosynthetic purple membrane from *Halobacterium salinarum* was demonstrated (Heberle and Pfitzner 2020).

AFM and even SNOM imaging of bacterial photosynthetic components has been performed decades ago (Worcester *et al.* 1990; Trudel *et al.* 2001). However, these earlier studies have concentrated on the photosynthetic complexes of anaerobic anoxygenic phototrophic bacteria. Technical advancements and structural understanding of the photosynthetic molecules have increased

immensely since these early studies. Nowadays, the detailed knowledge of individual components of the photosynthetic complex allows for easier analysis of the native membrane (Scheuring and Sturgis 2009). Therefore, SNOM imaging of native photosynthetic membranes with modern instruments and latest knowledge has a great potential of discovering new details on particular photosynthetic mechanisms. Research involving SNOM and photosynthetic membranes has focused mainly on the above-mentioned purple membranes (Heberle and Pfitzner 2020; Kanevche 2022). It would be intriguing to do similar measurements with the photosynthetic membranes of the here studied AAP species for a direct comparison of the aerobic and anaerobic mechanism. SNOM could enable live imaging of membrane and electron transfer dynamics during photosynthesis. While not yet in a native membrane, the photocurrent of the protein photosystem I was already measured using SNOM ten years ago (Gerster *et al.* 2012).

1.4 Aims of the studies

This work aimed to compare different approaches to identify and analyze AAP bacteria. Macro- and microscopic methods were developed and explored to detect and characterize bacteria by using spectroscopic imaging methods with an emphasis on the detection of near-infrared fluorescence of BChl a, present in AAP bacteria. The suitability of handheld and microscope-attached hyperspectral cameras for initial identification, as well as for further characterizations, has been briefly evaluated. Additionally, a new 3D-printed, low-cost detection system has been used for the identification of AAP bacteria colonies. This part of the work will ideally give insights into easily approachable detection and characterization methods which can be used for high-throughput screening to discover new AAP bacteria species.

The main focus of this work was the method development for the extraction and imaging of photosynthetic membranes on the molecular level. Photosynthetic

membranes are regarded one of the most complex structures in biology and still hold many secrets (Ruban and Johnson 2015). Despite a comprehensive literature research, data on membrane extractions from AAP bacteria is scarce. Yurkov and colleagues (1993) reported a successful photosynthetic membrane extraction from AAP bacteria involving a sucrose gradient separation as well as Kopejtka and colleagues (2020) using centrifugation steps and high-performance liquid chromatography. Here, previously published methods on the photosynthetic membrane extraction of anaerobic purple bacteria were adapted to the aerobic anoxygenic phototrophic species *Sphingomonas glacialis* strain S2U11 to investigate its particular photosynthetic complex and develop a working protocol for further studies with SNOM detection. The suspected separated membranes were analyzed spectroscopically and imaged using AFM. Ideally, here obtained AFM images will give direct insights into the shape, size and arrangement of the photosynthetic complex of *S. glacialis* in the photosynthetic membrane. Hopefully, the here developed methods will prove useful for similar extractions in the future.

This work could also be an important step towards imaging photosynthetic membranes with SNOM to combine AFM topography with the addition of localized, high resolution spectroscopic data. Future SNOM analysis may reveal new insights on the specific, localized light absorption and energy transfer of different molecules of the photosynthetic complex in the native membrane. Here, AFM imaging was performed in air, as it will be easier to start future SNOM studies in this imaging mode. However, the developed extraction protocol also enables imaging in liquid which would be very interesting to continue with.

At the current time, nobody at the University of Jyväskylä is working with bacteria membranes to the authors knowledge. This work aimed to explore the possibilities of available equipment and knowledge to extract and image bacteria membranes with AFM and scope the possibilities to later image the sample with SNOM. Similarly, the here described experiments involving AAP bacteria and

hyperspectral cameras for imaging were the very first attempts, aimed to scope the possibilities of using available equipment for new purposes.

Ideally, all here presented methods could be employed for the detection and characterization of different phototrophic bacteria species to discover individual differences in their photosynthetic complexes and enable further studies. Additionally, this work contributes to the better understanding of different photosynthesis types, such as anaerobic and aerobic bacterial photosynthesis.

2 MATERIALS AND METHODS

2.1 Materials

The *S. glacialis* strain S2U11 used for this experiment was originally isolated from the leaf endosphere of *Diapensia lapponica* by Riitta Nissinen in Kilpisjärvi, northern Finland (Nissinen et al., 2012). R2A medium and BD Bacto agar for cultivation of *S. glacialis* were sourced from Thermo Fisher Scientific (Waltham, MA, USA). HEPES buffer (≥ 99.5%, Ref. H3375) and n-Dodecyl β-D-maltoside (DDM, ≥ 98%, Ref. D4641) used in the membrane extraction were acquired from Sigma Aldrich (St. Louis, MO, USA). Sucrose (≥ 99%, Ref. 821713), used for the sucrose gradients was sourced from MP Biomedicals (Irvine, Ca, USA).

2.2 Methods

2.2.1 Low-cost fluorescence detection

The successful production of LH1 complexes in bacteria was always verified with a self-built, low-cost detection imager, which was inspired by a research-grade fluorescence imaging system used by Zeng and colleagues (2014). The 3D-printed imaging chamber holds each one consumer-grade white light-emitting diode (LED) and UV LED flashlight. There is a simple diffuser placed in front of the white light

to reduce strong reflections from the Petri dish. The diffuser was cut out of readily available surgical masks made of polypropylene fibers. A bottom drawer can be removed to insert a Petri dish for imaging (Figure 1). Surrounding light leakages were avoided by the black chamber. The employed 8-megapixel camera module PiNoir V2 (Raspberry pie, Cambridge, UK) ships without a hot mirror which allows it to record also the NIR region of the light. It was operated by a Raspberry Pie computer model 3 B+ (Cambridge, UK) and a custom software which enabled it to change acquisition time and gain to account for different light sources.

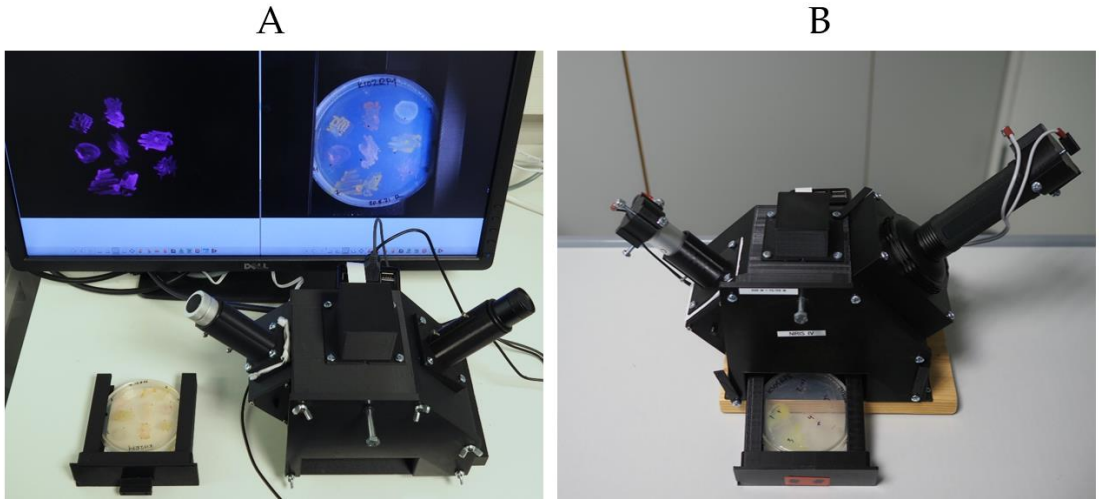

Figure 1 A) 3D-printed detection imager with manual light switches and 12 LED UV light illumination. Fluorescent imaging mode (left) and white light imaging mode (right) can be seen on the screen in the back. The Petri dish in the holder was removed from the device. Both versions have a similar 12 LED white light attached on the left and the UV light attached on the right. The camera sits on top while the bolt sticking out in the front holds a NIR filter which can be moved in front of the camera. The raspberry pie computer sits in a holder at the back of the box. **B)** A version of the imager with a 128 LED UV lamp and computer-controlled switches.

An 880 nm ± 8 nm bandpass filter (Model FB880-70 with FWHM = 70 ± 8 nm, Thorlabs, Newton, NJ, USA) can be engaged in front of the camera to restrict it to record only the expected fluorescence in the NIR region, from ~850 nm to ~900 nm (Figure 2). For detection of AAP bacteria colonies, UV-induced NIR fluorescence can be employed which verifies the presence of BChl a in the cells since it fluoresces at ~890 nm, in-vivo (Sebban and Moya 1983). For the fluorescence acquisition mode,

the white light is switched off, the UV light is switched on and the filter is pushed in front of the camera to only enable NIR light to reach the camera sensor (Figure 1 A and Figure 2 B & C). The imager was designed to also enable the recording of a reference white light image to count all colonies and assess their size, shape and color. For this, the white light is turned on, the filter is pulled away from the camera and a second picture is taken (Figure 2 A). During the whole procedure, the Petri dish stays in the same position and both flashlights remain at the same incident angle for every Petri dish which reduces the amount of variation caused by changing reflections and uneven lighting.

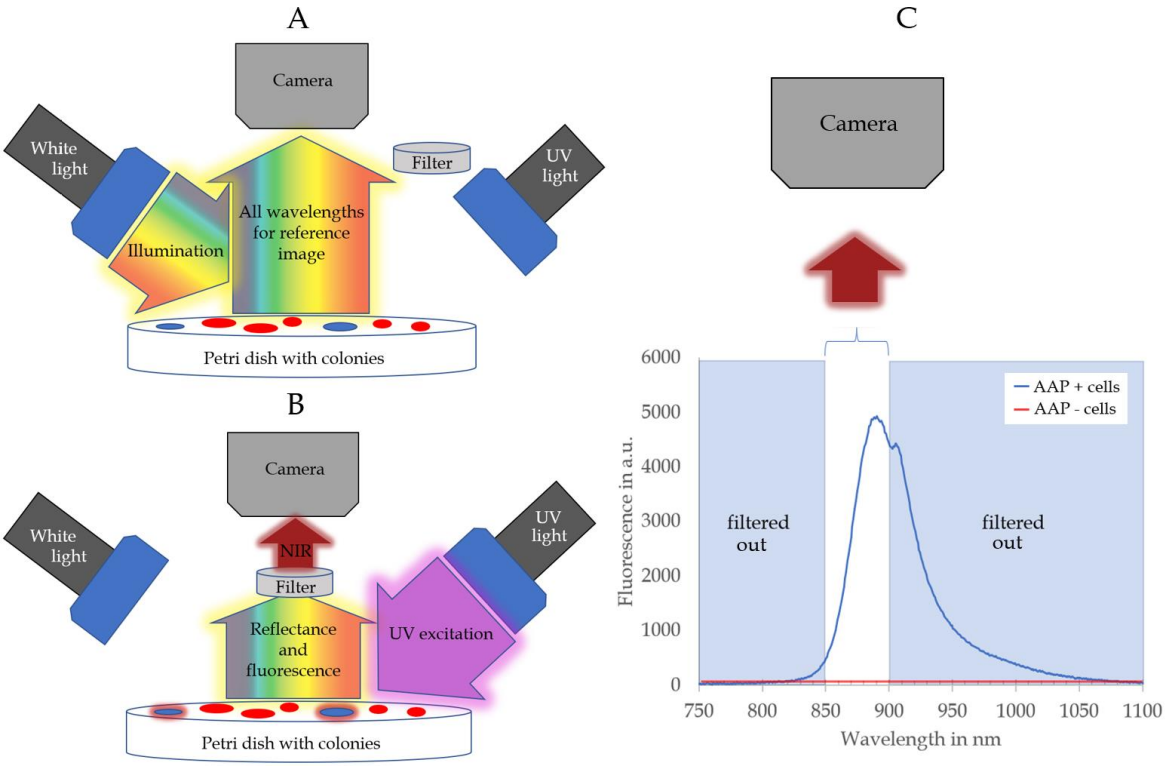

Figure 2 A) This scheme of the 3D-printed imager demonstrates the white light reference imaging. The white light excitation source is switched on, the filter is moved aside, and all wavelengths are recorded by the camera. **B)** During fluorescence imaging bacteria colonies are illuminated with UV light. The induced NIR fluorescence of AAP bacteria (marked in blue) passes the engaged filter and reaches the camera. **C)** Schematic UV light-induced fluorescence spectra of AAP bacteria (blue) with the approximate wavelength range passing through the bandpass filter to the camera. Bacteria without BChl a-containing photosynthetic complexes do not fluoresce in the NIR region under UV light excitation (red curve).

The set-up has undergone several alterations to improve its performance. The current set-up (September 2022) employs a 128 LED UV flashlight (Glossday, China) rated at 395 nm, powered by 6 AA batteries for the fluorescence mode and a much smaller, diffused white 12 LED flashlight for the regular imaging mode. Both lights are still cheap consumer-grade lamps to keep the price low and the acquisition easy. In the latest version of the imager, switches are controlled through the program, enabling the automation of light switches and image capture (Figure 1 B). Computer-controlled switches automatically turn on the correct lamp for the duration of the image acquisition when the program is run. This operation generally saved battery power and operation time. Previous versions were equipped with 12 LED UV flashlights which were manually operated (Figure 1 A). Also, a wired power supply for the UV flashlight was built to minimize power fluctuations caused by battery operation and heating of the LEDs. Petri dishes imaged with this device were always closed to ensure sterility and imaged from the bottom to provide an even surface without additional reflections between agar and lid. The imager remains highly customizable as the design is modular. The chamber can be easily re-printed and holders for different light sources, samples or cameras can be changed individually without having to re-design the whole chamber.

This fluorescence detection imager has been used to screen environmental samples for potential new AAP bacteria species. Depending on the sample type, there may be differences in the protocol. Extracts can be first concentrated by centrifugation steps and then plated in a dilution series to increase the chance of obtaining a suitable colony density with sufficient distance between individual colonies. Here, environmental samples extracted from the endosphere and phyllosphere of subarctic plants were cultivated to detect AAP bacteria. Extracts were plated and bacteria were grown for 3-5 days on half-strength R2A medium with 0.7% BD Bacto™ agar adjusted to pH 6.5 with HCl, on 92x16 mm polystyrene Petri dishes (Sarstedt, Nümbrecht, Germany). Cells were grown for three days at

room temperature after which they were placed in the fridge at +4 °C. Fluorescent signals of the bacteria colonies could be detected as soon as three days after plating. However, some colonies needed several weeks to gain sufficient fluorescence for detection.

2.2.2 Imaging with hyperspectral cameras

Macroscopic spectral imaging was performed with a Specim IQ hyperspectral imaging camera (Oulu, Finland) attached to a stand. For transmission and absorption measurements, the Petri dish was placed on a small fiber optic diffusion table (Model QVABL48M, Dolan-Jenner, Boxborough, MA, USA), connected to a halogen light source (Model DC-950, Dolan-Jenner, Boxborough, MA, USA) and imaged straight from above. The Petri dish was imaged without lid to decrease reflections. An image of the light diffuser plate without the Petri dish was used as a blank to calculate accurate transmission values across the entire image. In this set-up, transmittance was the recorded normalized spectral radiance between the blank white reference and a black reference. Absorption was then calculated as the negative logarithm (-log) of the measured transmittance. The Specim IQ recorded transmittance in ~ 3 nm intervals from 400 nm to 1000 nm.

For fluorescence imaging, a light source was aimed at the Petri dish surface to measure the spectra of the reflectance of the sample. An opaque glass diffuser placed in front of the light source helped to reduce reflections and create more even lighting across the Petri dish surface. The Petri dish lid was removed to reduce reflections. Different light sources were tried, including UV LED flashlights used in the 3D-printed imager, halogen and more powerful metal halide light sources (Models DC-950 & MH-100, Dolan-Jenner, Boxborough, MA, USA) used with a bandpass filter (Model FB590, Thorlabs, Newton, NJ, USA). Macroscopic fluorescence imaging of colonies on a Petri dish was briefly tested both with the Specim IQ (Oulu, Finland) and a VTT-Spectral imager-prototype 2 (Espoo, Finland). The VTT camera recorded fluorescence spectra from 605 nm to 990 nm in ~5 nm intervals.

Testing was also done with the same VTT-Spectral imager-prototype 2 (Espoo, Finland) attached to an upright Axio Scope.A1 microscope (Carl Zeiss, Oberkochen, Germany). Both fluorescence and absorption measurements were tested on a spot of *S. glacialis* cells on a glass slide, as well as individual cells. For more information on the general performance and characteristics of this prototype camera from VTT, refer to the recently published thesis from Leevi Lind (Lind 2021).

For all measurements with hyperspectral cameras, an area of ten-by-ten pixels around a selected center point was averaged to obtain the spectrum of a bacteria colony. The selected points were placed manually in the center of each colony or onto a reference area.

2.2.3 *S. glacialis* strain S2U11 cell cultivation for membrane extraction

50 µl glycerol stock of *S. glacialis* S2U11 stored at -20 °C were used to plate each 92x16 mm polystyrene Petri dish (Sarstedt, Nümbrecht, Germany). Cells were grown on half-strength R2A medium with 0.7% BD Bacto™ agar, adjusted to pH 6.5 with HCl. Colonies were grown for three days at room temperature after which they were placed in the fridge at +4 °C. Cells were then harvested after at least 7 but not more than 21 days in the fridge. Petri dishes were analyzed for NIR fluorescence with the aforementioned 3D-printed imager to ensure that sufficient amounts of photosynthetic membrane were produced.

2.2.4 Photosynthetic membrane extraction from *S. glacialis* strain S2U11

The membrane extraction protocol was inspired by the publication of Scheuring and Sturgis (2009) and Bahatyrova and colleagues (2004). Cells were harvested with a plating spatula and addition of Tris-HCl buffer (pH 7) to wash the agar surface and suspend the bacteria. For one batch, cells from five Petri dishes were suspended in a total of 30 ml Tris-HCl buffer (pH 7) to have a sufficient volume for the cell lyzer. Cells were broken with an Emulsiflex C3 homogenizer (Avestin, Ottawa, ON, Canada) in a single pass at 300 bar and collected into 50 ml centrifuge tubes on ice.

The lysate was then centrifuged at 20,000 g for 10 min at +4 °C using a Sorval RC 6+ centrifuge (Thermo Fisher Scientific, MA, USA) with a carbon rotor (Model F21S-8x50Y, Thermo Fisher Scientific, MA, USA) and acceleration and deceleration set to level 9. After centrifugation, the supernatant was carefully removed by pipetting. Approximately 600 µl was saved in each tube as the pellet and kept on ice. The pelleted lysate of 5 harvested plates was shared to two ultracentrifuge tubes. The pellet was first homogenized by pipetting and then mixed with the lowest sucrose concentration. The sucrose gradient was prepared right before the separation centrifugation, to obtain clear separation zones instead of continuous gradients. This might aid the formation of a more distinct band, since the membrane pieces may be of different size and with varying amounts of embedded proteins.

Different gradient steps were tested, ranging from 60% to 10% (w/w) sucrose in 50 mM HEPES buffer (pH 7.5) with 0.003%, 0.03% (w/v) and without n-Dodecyl β-D-maltoside as a detergent. Gradients were carefully filled into 14 x 89 mm ultra-clear™ ultracentrifuge tubes (Beckman Coulter, REF 344059) using the slowest setting of an electronic Eppendorf Multipette® (Hamburg, Germany) pipette with a 5 ml tip. Gradients were pipetted starting from the bottom with the highest concentration and raising the pipette tip continuously at the tube wall with each gradient addition. The successful gradient for membrane separation included steps of 50%, 45%, 40%, 30%, 20% and 10% (w/w) sucrose plus the addition of the sample mixed 1:2 with 10% (w/w) sucrose at the top. All gradients were 1.5 ml, except for the top one, which was added until it reached two millimeters under the opening of the tube, to avoid its collapse during centrifugation.

Finally, the filled ultracentrifuge tubes were weighed and equalized before 2 h centrifugation at 90,000 g and +4 °C with acceleration and deceleration set to slow. The ultracentrifuge model Optima L-90 K (Beckman Coulter, Brea, CA, USA) was used with the swinging bucket rotor SW41 Ti (Beckman Coulter, Brea, CA,

USA). After the separation centrifugation, the individual gradients were carefully transferred to individual 2 ml tubes and stored at +4 C.

2.2.5 Extract analysis

10 µl drops from each sucrose gradient were pipetted onto a glass slide and analyzed using the 3D-printed AAP bacteria detection imager introduced above. This way UV-induced NIR fluorescence in each fraction could be detected. After this initial analysis of UV-induced NIR fluorescence in the separated band, absorption as well as fluorescence spectra were measured from the extracted band and whole *S. glacialis* cells in water with a Spark® plate reader (Tecan, Männedorf, Switzerland) in 96 well plates. The absorbance of the extracted membranes and whole S2U11 *S. glacialis* cells was measured from 200 nm to 950 nm with 2 nm step size. A fluorescence spectrum was recorded with an excitation wavelength at 430 nm and emission recording with a step size of 2 nm. Additionally, excitation spectra at 895 nm with excitation wavelengths ranging from 310 nm to 850 nm with a 5 nm step size were recorded with the same imager and samples in order to find the optimal excitation wavelength and compare the spectra of the extract and whole cells. All measurements on the plate reader were done with one flash per measurement and 50 ms settle time between measurements. Absorption spectra were corrected for scattering using a fitted sextic polynomial function which was determined by selecting wavelength regions where absorption was assumed to be zero.

A higher quality UV-induced fluorescence spectra of both whole cells and the assumed extracted membranes were measured with a custom set-up. For this, material from both samples was dried on two different glass slides and mounted into the beam of a consumer-grade UV flashlight (Figure 3). Since it was early on detected that a battery powered flashlight is inconsistent in light output, a wired power supply was installed. A NIR-sensitive iDus InGaAs Spectroscopy CCD Camera (Andor Technology, Belfast, Ireland) was placed at a 90-degree angle to the UV lamp and the glass slide was placed in an angle so that incoming UV light

reflections were not directed towards the camera (Figure 3). The entire set up was shielded from surrounding light with matte black aluminum foil and cloth. Background images were taken without the UV light before every measurement so that the background was subtracted automatically. The acquisition time chosen for the dense and highly fluorescent whole cells was two seconds, while it was ten seconds for the more diluted extracted band. Generally, five measurements were done per sample. A mercury argon calibration lamp was measured after the samples and the wavelength range for all obtained data was corrected accordingly. For this, the deviation of the significant peaks from the reference lamp which were recorded to the known peaks was calculated. The resulting deviation term was applied to the previously acquired data and corrected accordingly.

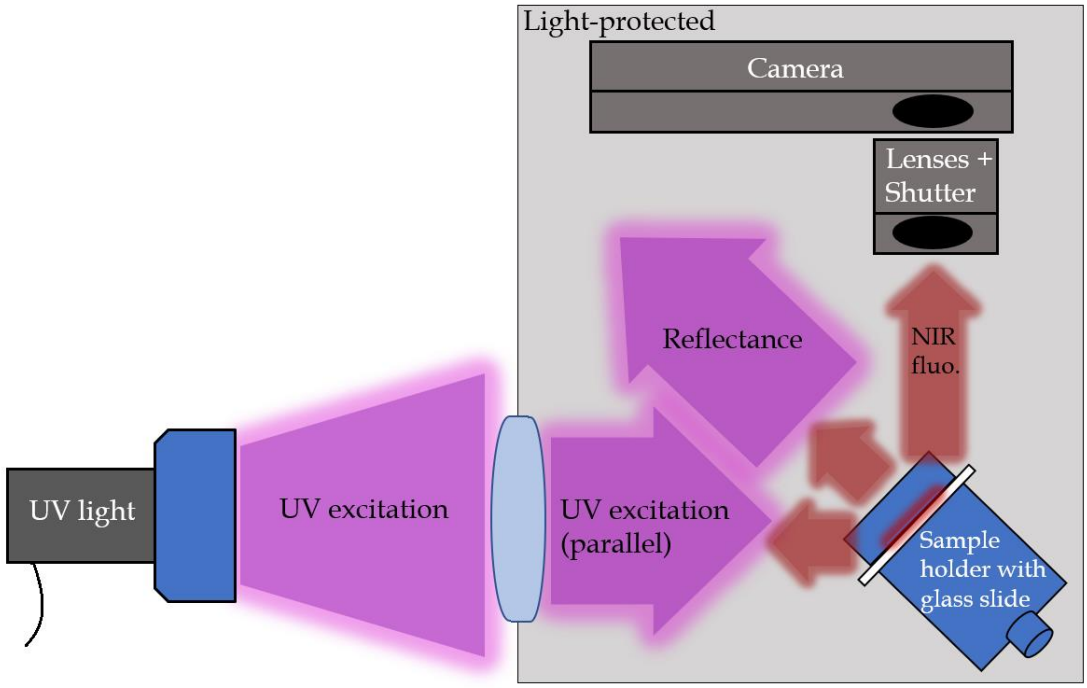

Figure 3 Simplified schematics of the fluorescence emission spectra set-up. A UV-flashlight was directed through a biconvex lens into a darkened box onto the sample glass slide clamped in a sample holder. The sample material was dried on the glass slide. The angle of the glass slide prevents reflections from entering the CCD camera.

2.2.5 Sample preparation for AFM imaging

Prior to sample absorption, two different sample preparations were tested to reduce the sucrose content. A dialysis protocol with Spectrum™ micro float-a-lyzer device (Thermo Fisher Scientific, Waltham, MA, USA) was investigated as well as a centrifugation protocol. For the dialysis protocol, the membranes were washed for 15 min with 10% EtOH, followed by six water rinses according to the manufacturer´s instructions. The device was then set to float in deionized water for 20 minutes at room temperature. The sample was then between the dialysis membranes and set to float in 75 ml of HEPES buffer (pH 7.5). The surrounding buffer was changed after 3,5 h with another 75 ml of HEPES buffer (pH 7.5). After a total of 14,5 hours, the sample was recovered from the dialysis device and used directly for imaging.

For the centrifugation purification protocol, 50 µl of sample were added to 1 ml of deionized water in a 1,5 ml test tube. The tube was then centrifuged at 20,000 g for 3 minutes in a pre-cooled rotor with a tabletop centrifuge model 5424 (Eppendorf, Hamburg, Germany). The supernatant was removed, and the procedure repeated. Then, the remaining pellet was dissolved in 50 µl deionized H_20 and imaged immediately with AFM.

2.2.6 AFM imaging

Samples were placed on freshly cleaved mica together with absorption buffer inspired by Scheuring & Sturgis (2009), consisting of 10 mM Tris-HCl, 150 mM KCl and 25 mM $MgCl_2$, adjusted to pH 7.6. The mica stack was initially adhered to a regular microscope glass slide with glue. Layers were freshly cleaved prior to sample absorption with the help of adhesive tape. Especially in the beginning, samples in their sucrose gradient without any additional preparation step were used for AFM imaging. Later, extracts were washed prior to the absorption as described above. Experiments were conducted with different sample-to-buffer ratios and altered incubation times, ranging from 10 to 40 minutes. Usually, 2 µl of

sample were pipetted into 40-80 µl of absorption buffer to cover the entire mica surface and incubated for 15 minutes. After incubation, the mica surface was washed at least six times with deionized water. For one washing step, the water was deposited on the surface, carefully mixed by repeated pipetting, and tapped off onto a paper towel from the edge of the glass slide. The samples were then dried using a nitrogen gun and kept in a clean Petri dish before imaging.

AFM imaging of the membrane was performed in tapping mode with forces set below 1 nN to avoid disruption or indentation of the soft membrane. In some cases, imaging with forces set as low as 0.099 nN was performed. It has been previously reported that forces larger than 2 nN may damage soft samples such as lipid membranes (Grandbois et al., 1998; Trudel et al., 2001). The images shown in this work were obtained with scan rates between 1.83 Hz for low magnification and 1.04 Hz for high magnification imaging. The peak force amplitude was set to either 200 nm or 150 nm.

AFM imaging of membranes was also attempted on silicon wafers instead of mica. Similar protocols were used by the group of Jussi Toppari which imaged biomolecules on silicon wafers in the same lab. Approximately 1,5 x 1,5 cm silicon wafers were treated with glow discharge plasma for 180 seconds using the model SC7620 (Quorum Technologies, Laughton, UK) to render the silicon surface more hydrophilic and negatively charged. The tested absorption buffers contained $MgCl_2$ in Tris-acetate-EDTA (TAE) buffer, in some cases together with $NiCl_2$. Final concentrations of 500 mM, 250 mM and 100 mM $MgCl_2$ were tested in TAE buffer. Additionally, 100 mM $MgCl_2$ together with 15 mM $NiCl_2$ was tested. The membranes were mixed 1:4 with absorption buffer and incubated for 30 minutes on silicon wafer freshly treated with glow discharge. Then, the sample was washed six times by tapping off deionized water from the wafer and dried either with a nitrogen gun or on air.

AFM imaging was done with the microscope Dimension Icon (Bruker, Billerica, MA, USA). Imaging in air was performed with Scanasyst-air cantilevers

with a silicon tip on a nitride lever (f_0: 70 kHz k: 0.4 N/m, Bruker, Billerica, MA, USA) and the *Peakforce QNM in Air* experiment mode of the microscope.

3 RESULTS

3.1 3D-printed AAP bacteria detection imager

The low-cost 3D-printed AAP detection imager proved very useful for high throughput screening of environmental samples. The development of bacterial fluorescence took between 3 days and 2 weeks on half-strength R2A medium, likely dependent on bacteria species and colony density on the Petri dish. AAP positive bacteria colonies with diameters above ~0.5 mm could be easily detected on plates with several hundred bacteria colonies (Figure 4). With the latest set-up, the entire process to image one Petri dish in normal and fluorescent mode took less than one minute. However, older versions of the imager took slightly longer due to weaker UV flashlights and manual light switches.

As expected, it was not possible to tell any differences between fluorescing colonies regarding the spectral analysis in the fluorescent mode due to the binary nature (positive/negative) of the result. Only NIR fluorescence intensity differences between colonies could be differentiated. However, fluorescence intensity was heavily affected by the uneven excitation illumination and was generally not a very valuable metric for the characterization of bacteria colonies with unknown cell counts. The regular white light picture obtained from the plate in the same position gave some indication on differing bacteria species based on colony color, shape and structure (Figure 4). Analyzing both pictures together was useful to choose the most promising candidates from a Petri dish with many AAP positives to increase chances for isolating the most diverse set of bacteria. Of course, it may be possible that different species have identical colony color, shape and structure or that bacteria belonging to the same species show different morphology. However, if

only a limited number of positive colonies are isolated, it makes sense to choose morphologically different colonies. Adding a black on white label on the Petri dish covered some of the area but made it possible to identify the sample even in the fluorescent mode (Figure 4 A). Additionally, some regular permanent markers were tested to be NIR fluorescent when excited with UV light, but not all. The right choice of marker could make markings disappear or appear during fluorescent imaging. Positive colonies were picked and re-plated for a second fluorescence verification (Figure 4 C). Selected AAP bacteria could be then sequenced, identified, and characterized further.

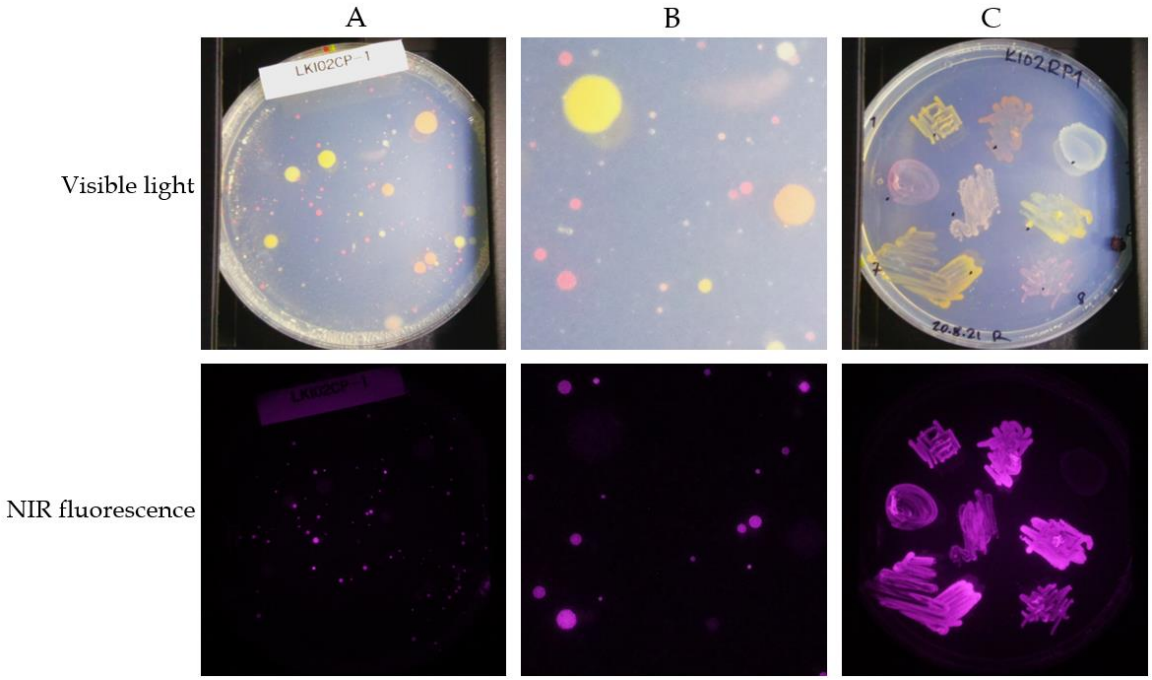

Figure 4 Images produced by the 3D-printed low-cost imager **A)** Shown are two pictures of the same Petri dish with an environmental sample. At the top, an image with white light excitation and unfiltered detection. At the bottom, NIR-filtered image with UV excitation. **B)** An area from the Petri dish shown in A but magnified in both imaging modes to demonstrate how small colonies can be detected **C)** Verification Petri dish showing selected isolates which were NIR fluorescence positive during a previous screening. The colony at the top-right corner of the image serves as a negative control. The purple hue in all fluorescence images was artificially added.

3.2 Hyperspectral camera for AAP bacteria detection

The performed tests with hyperspectral cameras for AAP detection and analysis were promising but proved also to be challenging. Imaging with the Specim IQ hyperspectral pocket camera resulted in simultaneous spectra recordings of all test colonies on a single Petri dish. Macroscopic imaging with the recording range of 400-900 nm was successful in transmission/absorption mode. A calibration image of the light table without the Petri dish improved the accuracy of the obtained data compared to using the default camera mode. The default mode picked a calibration point and assumed a completely even light intensity over the whole light table area, which was not the real scenario. However, ideally the blank image would have been recorded from an empty Petri dish filled with the same amount of culture medium to subtract its absorption from the bacteria absorption.

Differing colony thicknesses likely influenced the intensity measured in the transmission/absorption mode but should not have had a significant influence on peak positions, if the colony was not too thick to let light pass through. The same Petri dish was imaged using the 3D-printed imager and the hyperspectral camera Specim IQ. Without exception, all bacteria patches which were fluorescent in the detection with the 3D-printed imager showed an absorption peak at 872 nm, indicating the presence of BChl a molecules (Figure 5). Fluorescence intensities in the picture taken with the 3D-printed imager cannot be directly compared to the peak intensities of the hyperspectral camera due to uneven lighting in the fluorescent imaging and varying colony thicknesses in the absorption recording.

Along with other species, several samples of *S. glacialis* isolated from plants were present on the Petri dish. Interestingly, the shade of orange varied between the different samples, likely caused by differing carotenoid compositions (Figure 5 A). Additionally, the only non-fluorescent bacterium which was known to be *S. glacialis* was extracted from the leaf phyllosphere, while all other known *S. glacialis* samples were extracted from the endosphere and showed UV-induced NIR fluorescence (Figure 5).

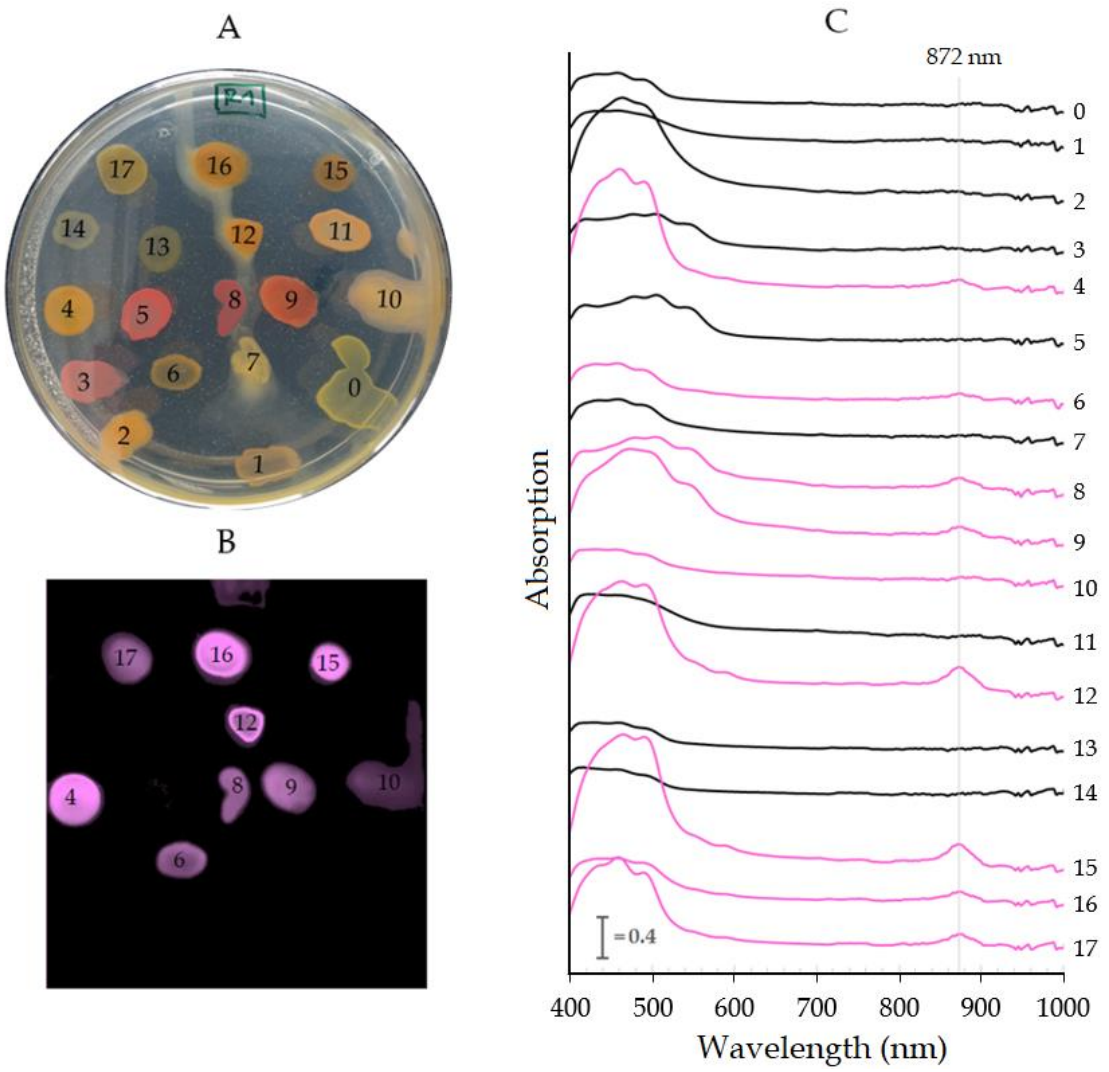

Figure 5 Comparison of bacteria analysis with **A)** white light, **B)** the fluorescence mode of the 3D-printed imager and **C)** results of the hyperspectral pocket camera Specim IQ. For the results of the hyperspectral camera, absorbance was calculated as -log of the transmittance. The shown spectra were averaged from 10x10 pixels manually placed on each colony. Numbers on the right of each spectrum correspond to numbers on the bacteria in A and B. All spectra of AAP positive bacteria detected with the 3D-printed imager in B have been colored pink in graph C for clarity. The majority of the isolates have been not sequenced. Bacteria on spots 17, 16, 15, 13, 12 and 4 have been sequenced to be >99% identical to the *S. glacialis* type strain and have been isolated from *Diapensia lapponica*. For number 10, it was 98,46% identical (data not shown, R. Nissinen, unpublished). All mentioned *S. glacialis* isolates were extracted from plant endosphere except for 13, which was isolated from the leaf phyllosphere.

Initial tests of fluorescence imaging with the Specim IQ hyperspectral camera indicated that a strong light source is needed as excitation light to result in sufficient fluorescence to be recorded. In the here tested set-up, it was not possible to obtain satisfactory results when imaging bacteria colonies on a Petri dish using strong halogen or metal halide light sources. In our hands, it was not possible to adjust the acquisition times or lighting in a way to produce satisfactory results.

However, macroscopic fluorescence imaging with the VTT-Spectral imager-prototype 2 produced spectra indicating NIR fluorescence. But recorded spectral data from all colonies on the Petri dish showed a clear NIR fluorescence peak between 890 and 895 nm while prior absorbance measurements and imaging with the 3D-printed device indicated that not all bacteria colonies show BChl a fluorescence (Figure 6 A). This meant that the fluorescence imaging with the VTT-Spectral imager-prototype 2 with the tested set-up was likely to be inaccurate. The false positives may have occurred due to fluorescent light reflections on AAP negative colonies coming from strongly fluorescent cells. Also here, as with all fluorescence imaging set-ups involving Petri dishes, surface reflections and even illumination across the plate were challenging.

Microscopic fluorescence analysis with the VTT-Spectral imager-prototype 2, attached to a Zeiss Axio Scope.A1 microscope, was possible when performing initial tests with patches of *S. glacialis* smeared to a glass slide (Figure 6 B). The area with bacteria showed a clear fluorescence peak at 890 nm while the reference empty area next to the bacteria showed no peak. However, transmission/absorption analysis with the same set-up and sample was only successful in the visible wavelength range. This was indicated by the sudden drop of signal after 700 nm (Figure 6 C). It was likely caused by internal coatings in the light path on the illumination end as this was the only thing that differed from the fluorescence imaging. For absorption/transmission measurements the light was coming from behind the sample while it was coming through the objective when doing reflectance/fluorescence imaging.

Imaging of single bacteria proved difficult, as the required shutter speeds to capture the fluorescence were too low to freeze the moving bacteria. For this reason, work with hyperspectral cameras attached to light microscopes was not continued. Other microscopic imaging techniques, such as confocal microscopy, were not considered due to the lack of sensors recording in the NIR region.

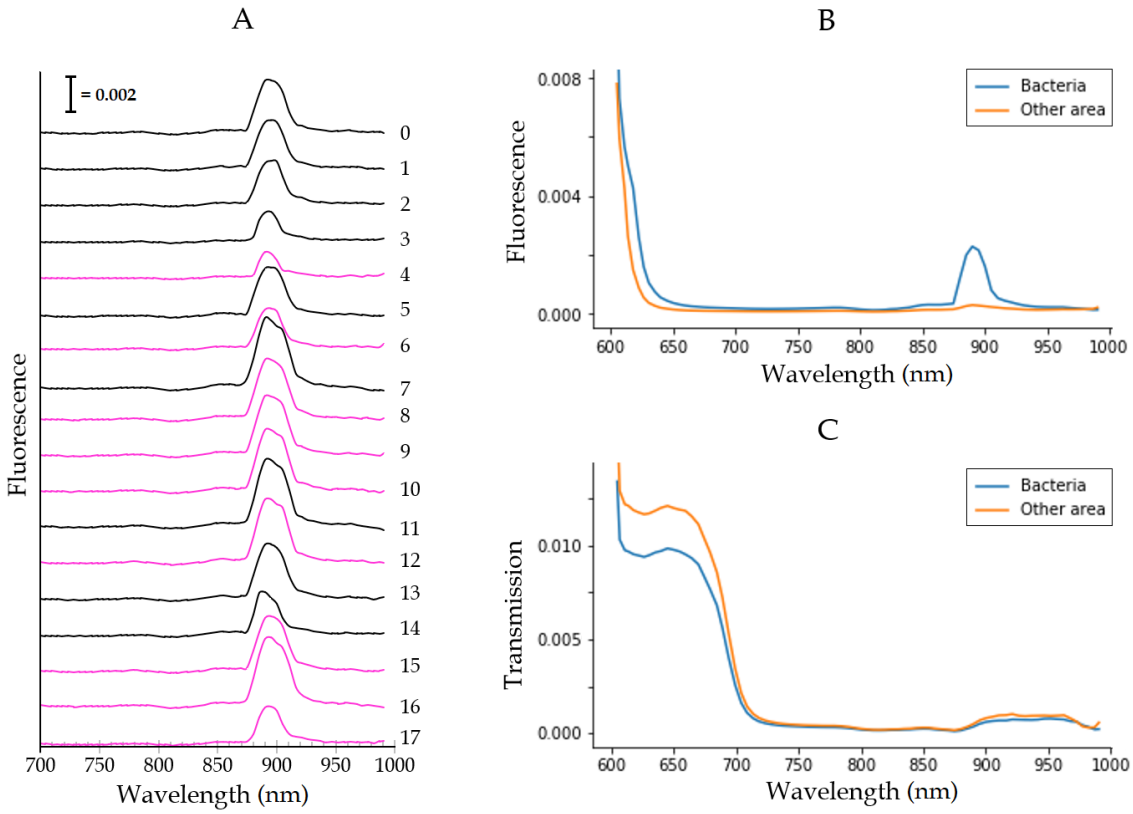

Figure 6 A) Fluorescence imaging results obtained with the VTT-Spectral imager-prototype 2 hyperspectral camera from the Petri dish shown in figure 5 A & B, displaying a consistent fluorescence peak between 890–895 nm across all sampling locations. The shown spectra were averaged from 10x10 pixels manually placed on each colony. The numbers next to the spectra on the right correspond to the labelled bacteria colonies in figure 5 A & B. Colony numbers with pink colored spectra have been previously identified as AAP positive with the 3D-printed fluorescence imager. **B)** Fluorescence spectra obtained with the same VTT camera mounted to a microscope. Sampling areas were on top of a dense layer of *S. glacialis* bacteria (blue) and an empty reference area (orange). **C)** Transmittance measured with the same set-up and sample as in B, except for the light source location. When the light source was set behind the sample for transmittance/absorption measurements, light beyond 700 nm would not reach the camera through both *S. glacialis* bacteria (blue) or an empty reference area (orange).

3.3 Extraction and AFM imaging of photosynthetic membranes

Sphingomonas glacialis cells from strain S2U11 were cultivated successfully from glycerol stock on half-strength R2A medium. Cells were observed with a regular light microscope to have a short rod shape and measured to be 1-3 μm in length (Figure 7 A). The aforementioned growing conditions including a dark refrigerated period resulted in the development of strong UV-induced NIR fluorescence, indicating the presence of photosynthetic membranes (Figure 7 B). The harvested suspension of orange *S. glacialis* cells, passed the pressure homogenizer without complications.

In the following ultracentrifuge separations, in which the highest concentration was 50% sucrose, most of the sample sedimented as a pellet to the bottom of the tube, leaving a clearly separated band at the edge between 45% and 50% (w/w) sucrose (Figure 7 C). Separation attempts which included 40%, 50% and 60% sucrose, but no separate 45% step, resulted in no visible separation. The entire sample formed a band between the edge of the gradient steps containing 50% and 60% sucrose (Figure 7 C). The UV induced NIR fluorescence analysis of the individual fractions revealed that the separated material was still fluorescent in the near-infrared region, indicating that it likely contained the photosynthetic membranes. The pellet was highly fluorescent, indicating that BChl a containing photosynthetic complexes were also present. This was likely caused mainly by unruptured cells. The use of 0.003% (w/v) n-Dodecyl β-D-maltoside in the sucrose gradient did not seem to have a significant effect based on the following AFM resulting in similar images.

The dialysis purification of the extract in its sucrose gradient was not successful, as the sample lost most of its fluorescence after the process. There were also no structures observed in the later AFM imaging from samples purified with dialysis. After this initial test, washing steps for the extracts were only done by centrifugation.

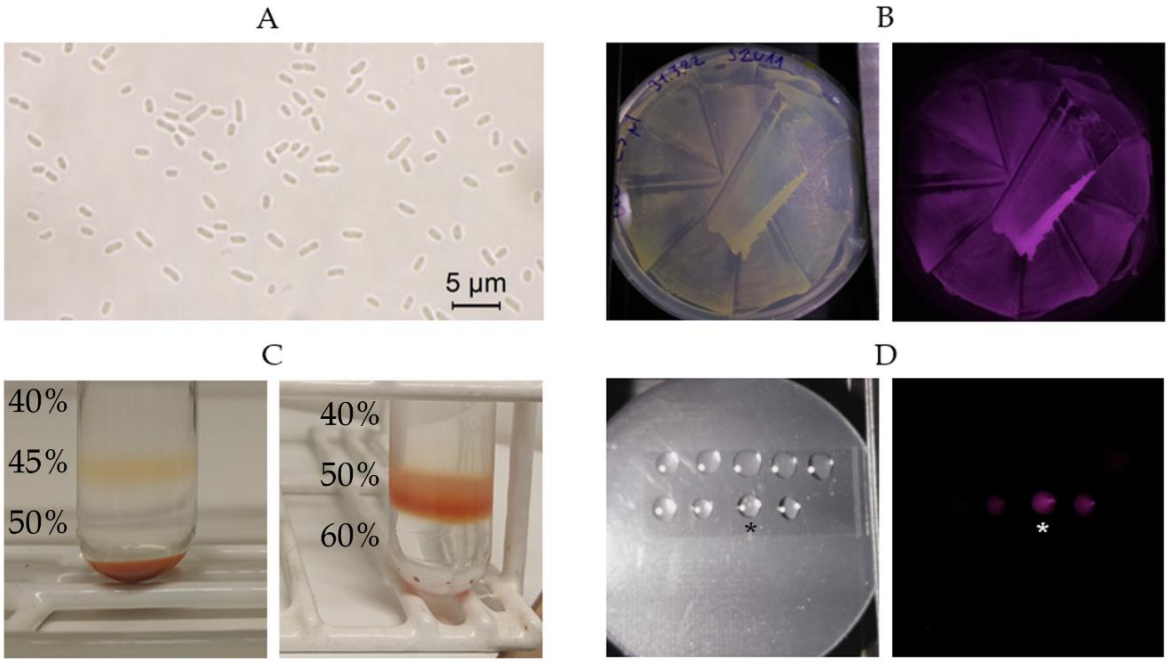

Figure 7 Membrane extraction from *S. glacialis* **A)** Light microscopy image of *S. glacialis* cells at 1000X magnification with immersion oil. **B)** Images from the 3D-printed imager demonstrate the density and NIR fluorescence of Petri dishes covered in *S. glacialis* for harvesting purposes. **C)** Results of the sucrose gradient separation of lysed *S. glacialis* cells. On the left, bottom layers were 40, 45 and 50% (w/w), while they were 40, 50 and 60% (w/w) sucrose on the right. **D)** Visualization of a rapid NIR fluorescence test of the different fractions after the sucrose gradient centrifugation using the 3D-printed imager. The drop marked with a star (*) originated from the center of the separated band shown on the left in image C. No sample drop was taken from the pellet into this image, as its strong fluorescence would have disturbed the accurate analysis of the less fluorescent fractions.

When measured with the Spark® plate reader, shape and position of the NIR absorbance and UV-induced fluorescence peak from both samples were very similar, indicating that components which absorb and fluoresce in those wavelengths were present in cells and extracted material (Figure 8 A). As mentioned earlier, BChl a in the LH1-RC complex of the photosynthetic membrane absorbs at around 870 nm and fluoresces at around 890 nm. The absorbance peaks were measured at ~878 nm , while the fluorescence peak was measured at ~886 nm with the plate reader (Figure 8 A).

The absorbance of the extracted membranes and whole S2U11 cells was measured from 200 nm to 950 nm. Absorption under 300 nm was very high due to the protein content of the samples and was therefore omitted from the analysis. The largest differences in peak shapes and relative intensity could be seen in the range from 400 nm to 550 nm, the region commonly referring to carotenoids in the sample. Different peak shapes and ratios in this region may indicate a different carotenoid composition. Additionally, the significantly higher peaks from whole cells show that more carotenoids are present, relative to the amount of BChl a (Figure 8 B).

The excitation spectra at 895 nm with excitation wavelength ranging from 310 nm to 850 nm revealed an optimal excitation wavelength at 370 nm in the UV-region. At the longer wavelength end of the measurement, a rising peak indicated another excitation wavelength in the NIR region, close to the fluorescence peak. However, crossover had to be avoided so fluorescence excitation spectra was only measured until 850 nm (Figure 8 B). Interestingly, it seemed that there is barely any energy transfer from carotenoids to BChl a, as there were no significant peaks in the fluorescence excitation spectra between 400 nm and 550 nm (Figure 8 B). Also, the peak at 370 nm in the fluorescence excitation spectra should line up with the absorption peak in the same region. The measurement resulted in slight mismatch of these two peaks indicating potential problems with the wavelength calibration of the device (Figure 8 B).

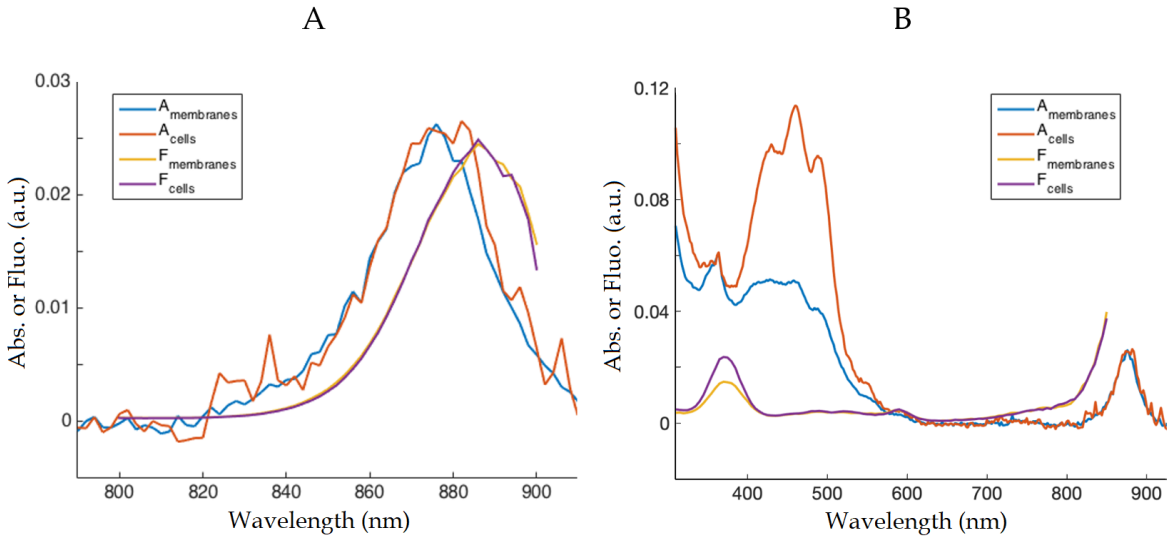

Figure 8 A) Absorbance and fluorescence emission spectra of *S. glacialis* strain S2U11 of both whole cells (red and purple) and extract (blue and yellow) in the NIR region, measured with a Spark® plate reader. Samples were excited with 430 nm for the fluorescence emission spectra. Each spectrum represents one measurement. Both spectra were measured with a step size of 2 nm. Data has been scaled to a similar peak height and is displayed in arbitrary units (a.u.). **B)** Absorbance and fluorescence excitation spectra from 300-900 nm of the same samples and measured with the same plate reader as A. Fluorescence excitation spectra was detected at 895 nm while the excitation wavelength was scanned from 300-850 nm with 5 nm step-size. Absorption spectra were corrected for scattering. Cells and extract were suspended in water.

Additionally to the plate reader analysis above, UV-induced fluorescence of both whole cells and the extracted band was measured with a high performance spectroscopy CDD camera, revealing the similarity of the NIR fluorescence peaks of whole *S. glacialis* cells and the extracted membranes in more detail. The main peak was at ~890 nm for both samples with a shoulder peak at ~905 nm. Shape and relative height between both peaks were similar for both samples indicating the presence of intact photosynthetic complexes (Figure 9).

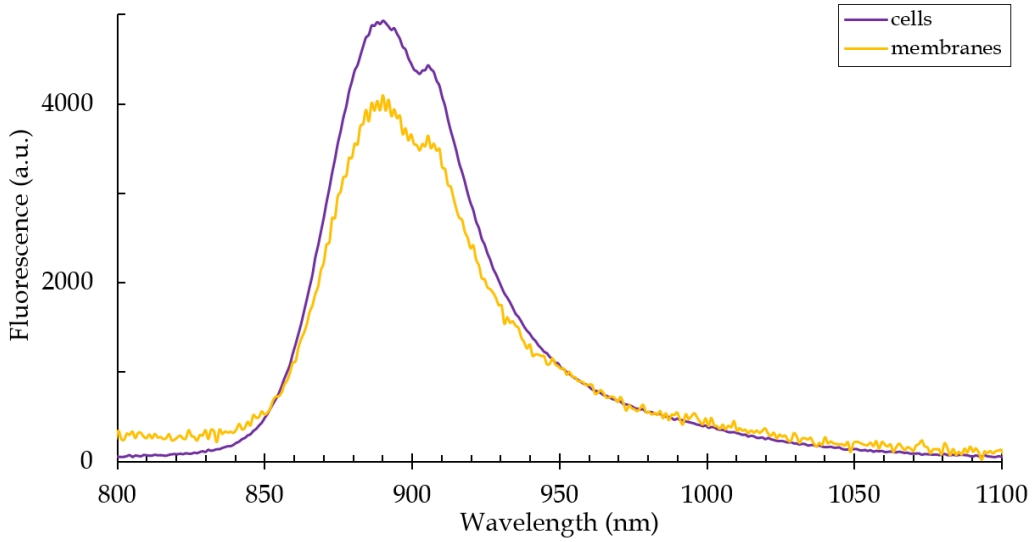

Figure 9 Averaged UV-induced NIR fluorescence spectra of dried separated membranes (yellow) and whole *S. glacialis* S2U11 cells (purple) on glass slides, measured with a spectroscopy CCD camera. The set-up was outlined in figure 3. Each depicted spectrum was averaged from 5 separate measurements. The data was corrected with the help of a mercury argon calibration lamp measured with the same camera. Data from both samples has been scaled to similar peak heights for comparison and is displayed in arbitrary units (a.u.).

For AFM imaging, the separated material was initially kept in the sucrose gradient and pipetted directly into the absorption buffer on freshly cleaved mica. After at least 10 minutes of incubation, repeated washing with deionized H_20 and subsequent drying, AFM imaging resulted in pictures of ~ 1 nm thin fragments with embedded, round structures (Figure 10). The diameter of these round structures varied between 15 – 30 nm and the height ranged between 4 – 8 nm (Figure 10 & 11). This observation could be made across several samples, from different separations on multiple days. An additional washing step of the sample prior to its addition did not significantly change the result. After several centrifugation washes, similar structures could still be observed (Figure 10). Longer incubation times of samples in the absorption buffer on mica seemed to increase the number of structures. While this seems intuitive, it was not always repeatable. Other factors such as minute differences in washing or mica surfaces may have had an impact as well.

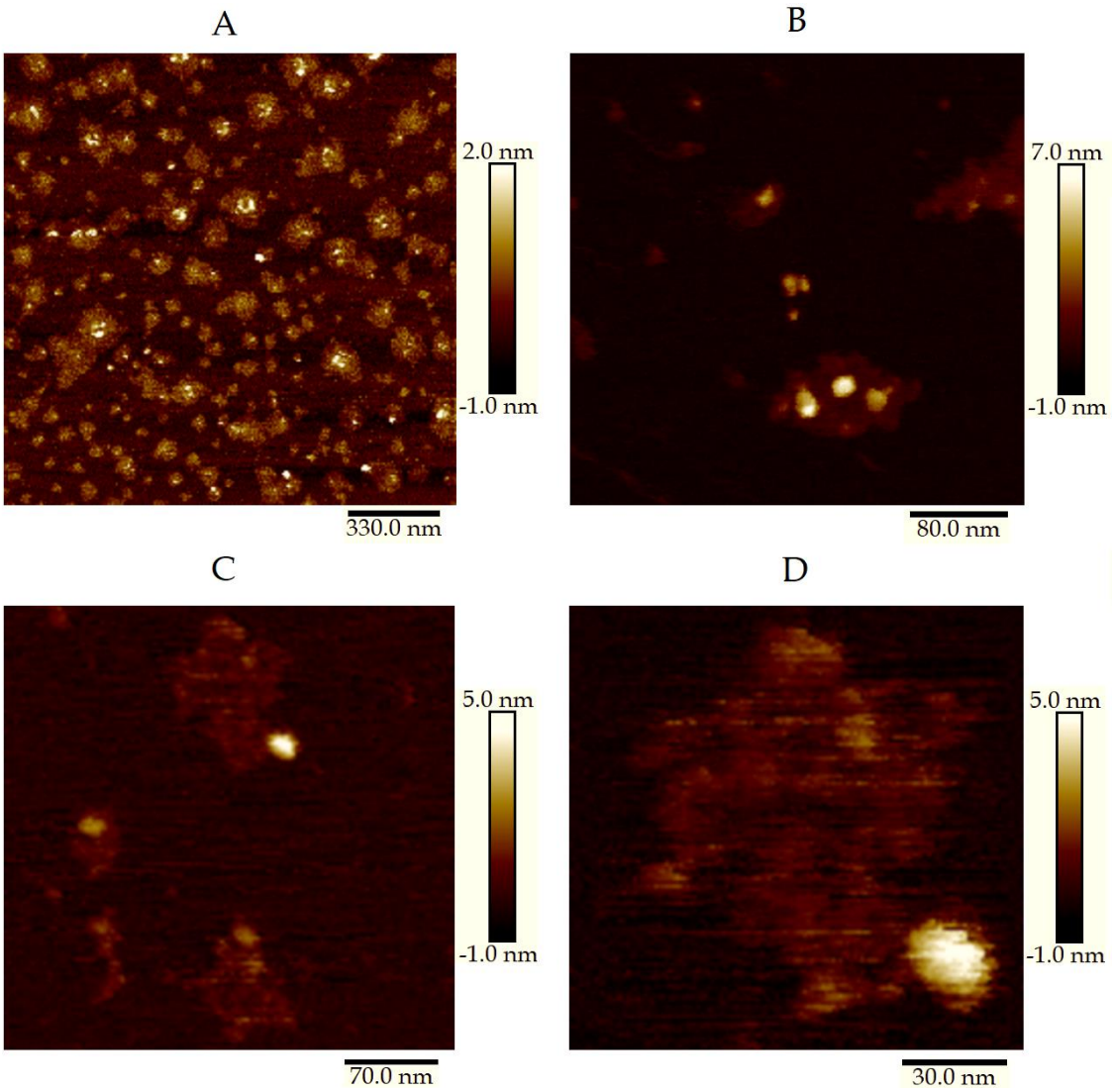

Figure 10 Various examples of AFM images of the *S. glacialis* extract on mica showing similar structures obtained with different sample preparations. **A)** Low magnification view displaying the amount and sizes of structures present in a sample after the centrifugation washing step. **B**) An example of three embedded structures grouped together and imaged at higher magnification. **C**) A single embedded structure in a sample which was only washed after absorption on mica. **D)** Higher magnification image of the same structure seen in figure C. All images were processed with plane fitting and flattening commands (both 1st order) using Bruker NanoScope Analysis software.

The observed structures were analyzed using Bruker NanoScope software. Heights and widths of the assumed membrane pieces and transmembrane proteins were measured. The surrounding assumed membranes were repeatedly ~1 nm

thick while the embedded protruding structures were between 4-8 nm high and 10-30 nm in diameter (Figure 10 & 11). The software allowed to display the AFM image with distinct colors associated to each height level (Figure 11 A). Tilted three dimensional models of the image showed effectively how the embedded structures were shaped like distinct cylinders with relatively sharp edges to the surrounding material (Figure 11 B). Drawn trajectories across the sample could be measured in even finer detail (Figure 11 C).

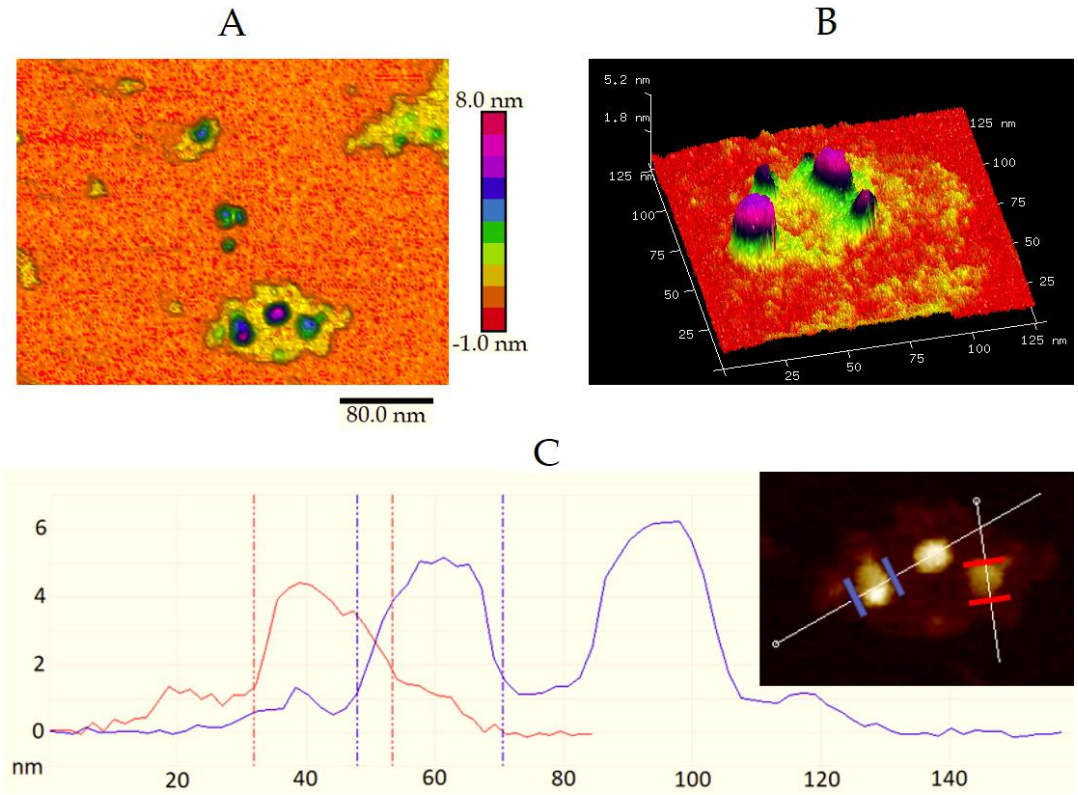

Figure 11 Height and width measurements of selected structures in AFM images from *S. glacialis* extract. **A)** Bruker´s NanoScope Analysis allowed for colored, clearly segmented separation of different heights in the nanoscale. Each color corresponds to a range of 1 nm. A 3D-like view simplifies the identification of heights. The same image was shown in Figure 10 B and can be used for comparison of the different viewing styles. **B)** It was possible to tilt and rotate 3D images freely to get a different perspective on the topography of the sample. **C)** Measuring the lengths and heights across selected trajectories. Trajectories were drawn to measure the dimensions of structures seen also in Figure A. The distance between the two blue and red bars was measured to be 23.14 nm and 22.07 nm, respectively. All images were processed with plane fitting and flattening commands (both 1st order) using Bruker NanoScope Analysis software.

While imaging on mica was generally successful, initial tests with silicon wafers did not work very well. When a nitrogen gun was used for drying the sample after the incubation time, artifacts in the blowing direction were visible, surrounding round structures with similar dimensions as seen on mica (Figure 10, 11 & 12). When the drying was done more carefully, the artifacts were not visible (Figure 12 B). There was no significant difference between the absorption buffers tested, including varying amounts of $MgCl_2$ and $NiCl_2$ in TAE buffer.

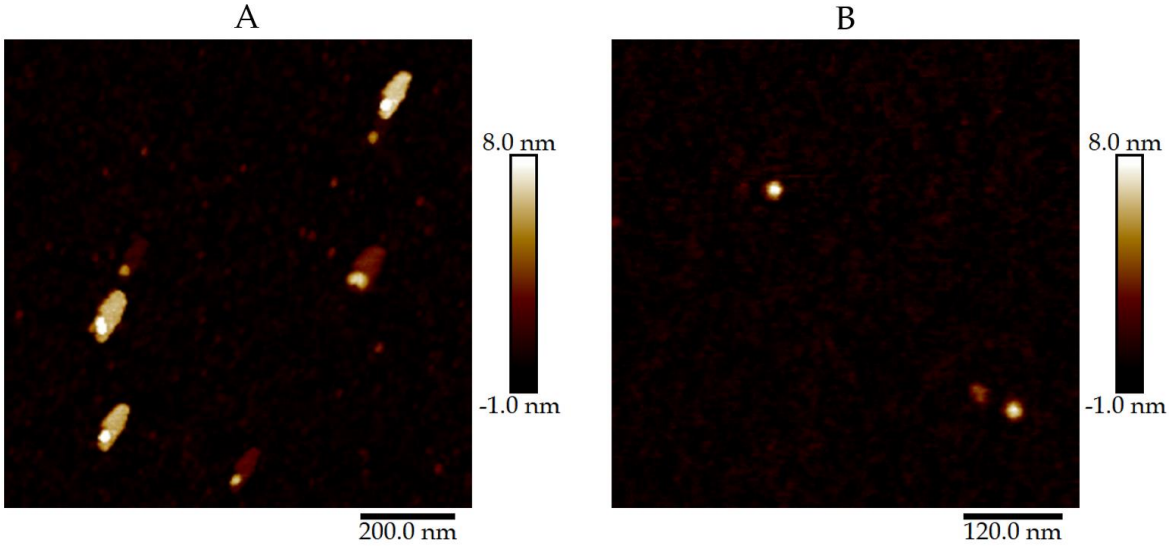

Figure 12 Different drying conditions affected AFM imaging results on silicon wafers. **A)** The extract was incubated for 30 minutes in 500 mM MgCl2 TAE buffer on silicon treated with glow discharge plasma. The sample was then washed 6 times and dried with a nitrogen gun. **B)** The AFM image was obtained from a similar sample, with similar preparation conditions than the sample in A, except for more careful drying in air.

4 DISCUSSION

4.1 Self-built AAP bacteria detection imager

The 3D-printed detection imager has proven immensely useful and easy to use. By now, many thousands of Petri dishes with bacteria extracted from the endosphere and phyllosphere of plants have been scanned for AAP bacteria. The devices are so cost efficient to assemble, that it was possible to send them to participating schools, along with sampling kits for AAP bacteria. Hopefully, available files and instructions will provide the opportunity for teachers, students and researchers to build similar detection devices in the future and use them for their own purposes. The modularity of the imager allows to use a variety of light sources with different wavelengths, different filters, cameras and sample holders, making it ideal for customisation. For example, it would be possible to use consumer-grade pocket cameras and flashlights to have a completely portable system. If NIR sensitivity is needed like in the here presented case of AAP bacteria detection, hot mirrors can be removed from the sensors by dedicated companies or following instructions from the internet. These so-called infrared conversions of cameras are commonly done for artistic purposes, but they would have a great potential for research applications, too.

The results showed that when the simple detection of organisms with a specific fluorescence is sufficient, a cheap camera with high quality filters can be a cost effective, fast and accurate solution. It was possible to show that similar looking colonies, or samples with the same species identification can have different results when tested for UV-induced NIR fluorescence.

While the current set-up works well for the simple detection of fluorescence, the uneven lighting prevents from comparing fluorescence intensities from different areas on the Petri dish. Future improvements could focus on creating more even lighting. Diffused ring lights around the camera or lenses in front of the lamps could work as well as using edge-lit light guide plates commonly used for monitor

backlights. For optimal comparability, also between measuring days over longer time frames, light sources should be ideally corded lamps. This would ensure stable and consistent light output. Additionally, it would be good to have a version of the imager with more easily exchangeable filters. Currently, the filter is not easy to access. However, this also serves a purpose as it is the most of expensive component of the imager and should not be handled without proper care. Ideally, filters could be threaded into an easily exchangeable module in the filter holder, thus eliminating the need for repeated screwing on and off. Replacing the filter could enable for example the detection of cyanobacteria with chlorophyll a which has fluorescence peaks in the 600-700 nm region (Grigoryeva and Chistyakova 2018). While the imager is not only applicable to AAP bacteria research, it has already helped to find several novel AAP bacteria species (R. Nissinen et al., unpublished).

Nowadays, 3D printing is widely accessible and suitable chambers with custom light source and sample holders can be designed and printed. However, not everybody is comfortable with computer-aided design (CAD) or has access to 3D printers. As long as the light sources, filter and camera are working for the application, a suitable chamber can be also built from wood or carboard, for example. It is even imaginable that functioning chambers could be built with commonly known toy construction bricks from Denmark. The CAD files with the design for the here presented imager could be made available in the future to enable free reproduction. As mentioned earlier, this could facilitate education and further research in several fields.

While this imager can help to detect expected fluorescence peaks, hyperspectral cameras additionally enable researchers to detect unexpected or altered peaks by recording a broad spectrum.

4.2 Hyperspectral cameras for absorbance and fluorescence analysis

Obtaining plausible fluorescence spectra of colonies on Petri dishes was not successful with the two tested hyperspectral cameras. While it was not possible with the here tested set-up to get any results with the Specim IQ compact camera, the fluorescence spectra obtained by the VTT-Spectral imager-prototype 2 were not satisfactory. All sampled spots showed a clear fluorescence peak for BChl a which was known to be not present in all. Nonetheless, all experiments involving hyperspectral cameras were initial test measurements. Altering light sources and their incident angles or generally the experimental set-up could significantly improve the results. The here presented results justify investing more time into experiments with hyperspectral cameras for the detection of fluorescent microorganisms.

The Specim IQ compact hyperspectral camera provided satisfactory results when measuring absorbance spectra of multiple bacteria spots on a whole Petri dish which would also be sufficient to detect AAP bacteria based on the characteristic absorbance spectrum of BChl a. However, so far it has not been tested with small colonies coming directly from environmental extracts. It is possible to generate a picture of the Petri dish showing absorbing areas which look similar to the ones obtained with the 3D-printed imager. However, in order to obtain the recorded spectrum at each spot of interest, the area has to be selected and the data retrieved from the selected pixels. Nevertheless, it may be possible to automate the selection process in the future. Hyperspectral imaging principally combined the high throughput of whole Petri dish imaging methods and analysing depth of spectroscopic methods. However, the cameras are expensive and less likely to be already present in research laboratories compared to fluorescence spectrometers. High-throughput processing coupled with absorption and fluorescence spectra can also be achieved with advanced plate readers. One large advantage of the hyperspectral cameras over plate readers is that they can be employed on Petri dishes and do not require liquid cultures or separately prepared cell suspensions.

The hyperspectral camera enables a non-invasive analysis of spectra from bacteria colonies since it doesn´t require any removal of cells from the colony. Additionally, it may be possible to detect and analyse larger structures of microorganisms, such as biofilms, directly in the environment.

4.3 Photosynthetic membrane extraction and AFM imaging

The extraction of clearly separated material from *S. glacialis* S2U11 cells with the help of a homogenizer and a sucrose density gradient was successful. The here presented results show that the infrastructure and all necessary equipment is available at the University of Jyväskylä to continue research in this direction. The clear separation band and similar shape of fluorescence emission spectra measured from the extract and whole cells indicated that the purification process yielded separated intact photosynthetic complexes in their native membranes.

While it is not possible to be entirely certain, structures observed with AFM from these extracts were likely photosynthetic membranes. Membrane-embedded LH1 surfaces in purple bacteria have been previously reported to be about 6 nm high with the central RC being about 7 nm high when imaged with an AFM in liquid (Scheuring and Sturgis 2009). Purified LH1-RC complexes of closely related *Sphingomonas* strain AAP5 were measured to be around 12 nm in diameter with a transmission electron microscope (Kopejtka et al. 2020). These dimensions fit to the observed structures, as the here measured heights were mostly identical and the diameters slightly larger. The here measured outer diameters of suspected LH1-RC complexes were measured to be between 15 – 30 nm from AFM images. Due to the nature of AFM, measured sizes in the X and Y direction may be larger than the true size of the structure. This is due to the tip shape and size, more accurately the sidewall angles and tip apex radius. Generally, if the structure has sharp edges they will be rounded and if has big step heights they appear slanted because the tip is not small enough to trace these features accurately. The smaller the recorded

structures are compared to the tip size, the greater is this effect. While the manufacturer states that the nominal tip radius for scanasyst-air tips is 2 nm, it can have a tip radius of up to 12 nm, according to Bruker. Wear or build-up may increase the tip size additionally, so it is reasonable to assume that the here measured structures with 15 – 30 nm outer diameter can be the size of previously reported LH1-RC complexes. Additionally, it is possible that the here measured membrane-embedded complexes have slightly different dimensions than the purified ones reported in the literature (Kopejtka *et al.* 2020).

Even in bigger pieces of the supposed photosynthetic membrane, only few complexes could be observed in the same piece. This corresponds well with the previously reported lower density of complexes in AAP bacteria compared to their anaerobic counterparts (Selyanin *et al.* 2015). Previous studies of photosynthetic membranes of anaerobic purple bacteria with AFM showed much denser packing of LH1-RC complexes (Bahatyrova et al. 2004; Scheuring and Sturgis 2009). One concerning observation was the thickness of only ~1 nm of the assumed bilayer membrane surrounding the LH1-RC complexes. Previously, bilayer membranes have been reported to measure ~4 nm, purple membranes even ~5 nm with an AFM in liquid (Müller et al. 1995; Unsay et al. 2015). It is possible that drying of the bilayer in the here tested protocol decreases the thickness of the bilayer. However, it cannot be excluded that the here observed supposed membranes were remnants from the sucrose gradients, despite the thorough washing steps. Initial, unsuccessful tests have been conducted to image the membranes in liquid (data not shown) in order to compare hydrated samples to dried ones. If similar dry samples are taken to SNOM in the future, fingerprint infrared spectra could ideally identify the composition of the surrounding structures. Similar membrane extractions have been mostly reported from anaerobic purple bacteria. Currently, it is not clear to what extend AAP bacteria possess similar internal photosynthetic membranes. It has been hypothesized that AAP bacteria may not need significant amounts of internal photosynthetic membrane, as their numbers of light-harvesting complexes is much lower (Yurkov and Beatty 1998). The extraction and imaging of internal

membranes from AAP bacteria species could therefor help to gain insights on the extent and arrangement of internal photosynthetic membranes.

AFM imaging in air was an initial step towards the imaging with SNOM since it both utilizes cantilevers and requires similar sample preparation. SNOM would allow the combination of topographic measurements with AFM and spectroscopic analysis, for example with Fourier transform infrared (FTIR) or Raman spectroscopy far beyond the conventional diffraction limit. Other absorption buffers and preparation conditions will be tested for AFM and SNOM imaging on silicon wafers since the here tested variations were not successful. The results indicated that the protein complexes may have adhered to the silicon wafer, while the membrane or surrounding structure, usually present when imaging on mica, was not visible. It is also possible that the absorption buffer was not suitable for membrane applications and disrupted the bilayer even before the incubation time. The here tested variations were initial tests and more buffer conditions on silicon wafers will be tested in the future. One first step will be to replace the TAE-$MgCl_2$ buffer with Tris-KCl-$MgCl_2$ buffer, similar to the one working on mica. Also, recent communications with an expert from the field revealed that gold layers have been proven to be a suitable substrate for purple membrane imaging with SNOM (Pfitzner *et al.* 2018; Giliberti *et al.* 2019; Kanevche 2022).

4.4 Additional analysis of *S. glacialis* strain S2U11 cells and extract

The absorption spectra of whole *S. glacialis* S2U11 cells and extracts obtained with sucrose gradient separations indicated that there are more and possible other carotenoids in whole cells based on the differences in peaks between 460-550 nm. This is plausible as it is assumed that not all carotenoids are located in the photosynthetic membrane. For example, they have been shown to be vital for maintaining fluidity of stability of membranes in general, especially in psychrotolerant bacteria (Subczynski *et al.* 1992; Jagannadham *et al.* 2000). It has also

been shown in the AAP species *Roseococcus thiosulfatophilus* and *Erythromicrobium ramosum*, that the majority of carotenoids were not bound to the photosynthetic complexes (Yurkov *et al.* 1993). Generally, the absorption spectra compare well with previously published spectra of other AAP bacteria and the closely related strain AAP5 (Yurkov and Beatty 1998; Kopejtka et al. 2021). The NIR absorption peak measured with the hyperspectral camera at 872 nm is identical to the one reported by Kopejtka and colleagues (2021) for the strain AAP5. It is likely that the plate reader was not optimally calibrated which resulted in a slightly different absorption peak. This theory is supported by the slight mismatch of the 370 nm peak in the fluorescence excitation spectra and the corresponding peak in the absorption spectra. The spectroscopic analysis of the closely related AAP5 cells determined the NIR fluorescence peak at 886 nm, while it was measured here to be at 890 nm for the strain S2U11 (Kopejtka et al., 2021).

Interestingly, the fluorescence excitation spectra of both extract and whole *S. glacialis* S2U11 cells indicated that there is no significant energy transfer from carotenoids to BChl a. This type of excitation transfer has been repeatedly reported for anaerobic purple bacteria (Krueger *et al.* 1998; Damjanović *et al.* 1999). Kolber and colleagues (2001) noted that also their sample of marine AAP bacteria showed carotenoids being involved in the excitation transfer to reaction centres based on a similar fluorescence excitation spectrum measurement as presented here. However, they hypothesized a connection of the higher penetration depths of light which excites carotenoids (460-550 nm) through water compared to that of NIR light. This may explain why excitation transfer of carotenoids to BChl may be more important in aqueous environments. Accordingly, similar energy transfer has been reported for other aquatic AAP species such as *Roseobacter* strain OBYS0001 or *Roseobacter denitrificans* (Sato Takabe *et al.* 2012; Šlouf *et al.* 2012; Sato-Takabe *et al.* 2014).

Since the *S. glacialis* strain S2U11 was isolated from the inside of plants, a lot of light which could be absorbed by carotenoids is absorbed by chlorophylls of the plant before it can reach the bacteria. The here presented results suggest that the

cells of the *S. glacialis* strain S2U11 contain a lot of carotenoids but their primary function may be protection from radiation-induced cell damage through quenching of reactive singlet oxygen and BChl a triplets, which is important for aerobic phototrophic organisms (Šlouf *et al.* 2012). This makes sense, as bacteria in and on plants are expected to be exposed to much stronger sunlight than bacteria in aquatic environments, due to the reflection and light absorption of water. However, roles of carotenoids in *S. glacialis* were not among the main questions for the here presented data. Future experiments with more measurements and altered experimental conditions may be helpful to gain further insides. Roles of carotenoids also likely change depending on growing conditions and here only one sample was tested. For example, it has been proposed that carotenoids involved in photosynthesis can be particularly helpful for starving cells (Sato-Takabe *et al.* 2014; Yurkov and Hughes 2017).

5 CONCLUSIONS

The aim of there here presented study was to test and compare available devices to detect and characterize AAP bacteria. The core of this work was method development, as most of the here shown experiments and measurements have not been tested at this university before. The results show clearly that the new 3D-printed detection is convenient and useful for AAP bacteria detection and may be of use for other fluorescence detection applications. It has also been demonstrated that the available infrastructure for work with photosynthetic membranes exists at this university. Extracts resembling photosynthetic membranes could be extracted from the *S. glacialis* strain S2U11 and analyzed spectroscopically and with AFM.

Aside from the positive experience with accurate absorbance spectra of AAP bacteria, experiments with hyperspectral cameras resulted in a new connecting link between the spectral imaging laboratory and researchers working on phototrophic

bacteria and photo-active proteins, which hopefully results in future collaborations. Similarly, AFM has been rarely used for biological research at this facility and not at all with native membranes. This work provides first guidance from sample preparation to AFM imaging settings for future work in this direction. Hopefully, it will be possible to utilize the insights gained here to move forward to improve AFM imaging of biological samples and use SNOM with these type of samples in the future.

ACKNOWLEDGEMENTS

The work gathered in this thesis has been supported by a number of people who I would like to thank. I want to thank Janne Ihalainen and Jussi Toppari for being my supervisors and providing support and guidance when needed. I am also very grateful for the help and advice I received from Heini Järvinen, Johannes Parikka and Kosti Tapio with AFM imaging and sample preparation. Many thanks to Ilkka Pölönen and Pauliina Salmi from the spectral imaging lab for their help with the hyperspectral cameras. Thank you, Heikki Häkkänen, for guidance during spectroscopic measurements and for designing and building the 3D-printed detection imager discussed in this thesis. Many thanks also to Riitta Nissinen, for providing me with *Sphingomonas glacialis* stock and helpful suggestions along the way. Thank you, Alli Liukkunen, for helping me find and operate lab equipment during the membrane extraction experiments.

REFERENCES

Arrigoni S., Turra G. & Signoroni A. 2017. Hyperspectral image analysis for rapid and accurate discrimination of bacterial infections: A benchmark study. *Computers in Biology and Medicine* 88: 60–71.

Atamna-Ismaeel N., Finkel O., Glaser F., Mering C. von, Vorholt J.A., Koblížek M., Belkin S. & Béjà O. 2012. Bacterial anoxygenic photosynthesis on plant leaf surfaces. *Environmental Microbiology Reports* 4: 209–216.

Bahatyrova S., Frese R.N., Siebert C.A., Olsen J.D., Werf K.O. van der, Grondelle R. van, Nlederman R.A., Bullough P.A., Otto C. & Hunter C.N. 2004. The native architecture of a photosynthetic membrane. *Nature 2004 430:7003* 430: 1058–1062.

Beatty J.T. 2002. On the natural selection and evolution of the aerobic phototrophic bacteria. *Photosynthesis Research* 73: 109–114.

Berweger S., Nguyen D.M., Muller E.A., Bechtel H.A., Perkins T.T. & Raschke M.B. 2013. Nano-chemical infrared imaging of membrane proteins in lipid bilayers. *Journal of the American Chemical Society* 135: 18292–18295.

Binnig G., Quate C.F. & Gerber C. 1986. Atomic force microscope. *Physical Review Letters* 56: 930–933.

Boeuf D., Cottrell M.T., Kirchman D.L., Lebaron P. & Jeanthon C. 2013. Summer community structure of aerobic anoxygenic phototrophic bacteria in the western Arctic Ocean. *FEMS Microbiology Ecology* 85: 417–432.

Busse H.J., Denner E.B.M., Buczolits S., Salkinoja-Salonen M., Bennasar A. & Kämpfer P. 2003. Sphingomonas aurantiaca sp. nov., Sphingomonas aerolata sp. nov. and Sphingomonas faeni sp. nov., air- and dustborne and Antarctic, orange-pigmented, psychrotolerant bacteria, and emended description of the genus Sphingomonas. *International Journal of Systematic and Evolutionary Microbiology* 53: 1253–1260.

Cepáková Z., Hrouzek P., Žišková E., Nuyanzina-Boldareva E., Šorf M., Kozlíková-Zapomělová E., Salka I., Grossart H.P. & Koblížek M. 2016. High turnover rates of aerobic anoxygenic phototrophs in European freshwater lakes. *Environmental Microbiology* 18: 5063–5071.

Chang C.-I. 2003. *Hyperspectral Imaging: techniques for spectral detection and classification (Vol. 1)*. Springer US.

Cohen-Bazire G., Sistrom W.R. & Stanier R.Y. 1957. Kinetic studies of pigment synthesis by non-sulfur purple bacteria. *Journal of cellular and comparative physiology* 49: 25–68.

Csotonyi J.T., Swiderski J., Stackebrandt E. & Yurkov V. 2010. A new extreme environment for aerobic anoxygenic phototrophs: biological soil crusts. *Advances in experimental medicine and biology* 675: 3–14.

Damjanović A., Ritz T. & Schulten K. 1999. Energy transfer between carotenoids and bacteriochlorophylls in light-harvesting complex II of purple bacteria. *Physical Review E* 59: 3293.

Delmotte N., Knief C., Chaffron S., Innerebner G., Roschitzki B., Schlapbach R., Mering C. von & Vorholt J.A. 2009. Community proteogenomics reveals insights into the physiology of phyllosphere bacteria. *Proceedings of the National Academy of Sciences of the United States of America* 106: 16428–16433.

ElMasry G. & Sun D.W. 2010. Principles of Hyperspectral Imaging Technology. *Hyperspectral Imaging for Food Quality Analysis and Control*: 3–43.

Fleischman D. & Kramer D. 1998. Photosynthetic rhizobia. *Biochimica et Biophysica Acta* 1364: 17–36.

Galachyants A.D., Krasnopeev A.Y., Podlesnaya G.V., Potapov S.A., Sukhanova E.V., Tikhonova I.V., Zimens E.A., Kabilov M.R., Zhuchenko N.A., Gorshkova A.S., Suslova M.Y. & Belykh O.I. 2021. Diversity of aerobic anoxygenic phototrophs and rhodopsin-containing bacteria in the surface microlayer, water column and epilithic biofilms of lake baikal. *Microorganisms* 9: 842.

George D.M., Vincent A.S. & Mackey H.R. 2020. An overview of anoxygenic phototrophic bacteria and their applications in environmental biotechnology for sustainable Resource recovery. *Biotechnology Reports* 28: e00563.

Gerster D., Reichert J., Bi H., Barth J. v., Kaniber S.M., Holleitner A.W., Visoly-Fisher I., Sergani S. & Carmeli I. 2012. Photocurrent of a single photosynthetic protein. *Nature Nanotechnology 2012 7:10* 7: 673–676.

Giliberti V., Polito R., Ritter E., Broser M., Hegemann P., Puskar L., Schade U., Zanetti-Polzi L., Daidone I., Corni S., Rusconi F., Biagioni P., Baldassarre L. & Ortolani M. 2019. Tip-Enhanced Infrared Difference-Nanospectroscopy of the Proton Pump Activity of Bacteriorhodopsin in Single Purple Membrane Patches. *Nano Letters* 19: 3104–3114.

Gonçalves R.P., Bernadac A., Sturgis J.N. & Scheuring S. 2005. Architecture of the native photosynthetic apparatus of Phaeospirillum molischianum. *Journal of Structural Biology* 152: 221–228.

Griffiths M., Sistrom W.R., Cohen-Bazire G. & Stanier R.Y. 1955. Function of Carotenoids in Photosynthesis. *Nature 1955 176:4495* 176: 1211–1214.

Grigoryeva N. & Chistyakova L. 2018. Fluorescence Microscopic Spectroscopy for Investigation and Monitoring of Biological Diversity and Physiological State of Cyanobacterial Cultures. *Cyanobacteria*.

Grondelle R. van, Dekker J.P., Gillbro T. & Sundstrom V. 1994. Energy transfer and trapping in photosynthesis. *Biochimica et Biophysica Acta (BBA) - Bioenergetics* 1187: 1–65.

Heberle J. & Pfitzner E. 2020. Infrared scattering-type scanning near-field optical microscopy of biomembranes in water. *Journal of Physical Chemistry Letters* 11: 8183–8188.

Imhoff J.F. 2017. Diversity of Anaerobic Anoxygenic Phototrophic Purple Bacteria. *Modern Topics in the Phototrophic Prokaryotes: Environmental and Applied Aspects*: 47–85.

Jagannadham M. v., Chattopadhyay M.K., Subbalakshmi C., Vairamani M., Narayanan K., Rao C.M. & Shivaji S. 2000. Carotenoids of an Antarctic psychrotolerant bacterium, Sphingobacterium antarcticus, and a mesophilic bacterium, Sphingobacterium multivorum. *Archives of Microbiology 2000 173:5* 173: 418–424.

Kanevche K. 2022. IR Near-field Nanoscopy and Spectroscopy of Cells and Soft Matter.

Kim M.K., Schubert K., Im W.T., Kim K.H., Lee S.T. & Overmann J. 2007. Sphingomonas kaistensis sp. nov., a novel alphaproteobacterium containing pufLM genes. *International Journal of Systematic and Evolutionary Microbiology* 57: 1527–1534.

Koblížek M., Mašín M., Ras J., Poulton A.J. & Prášil O. 2007. Rapid growth rates of aerobic anoxygenic phototrophs in the ocean. *Environmental Microbiology* 9: 2401–2406.

Kolářová E., Medová H., Piwosz K. & Koblížek M. 2019. Seasonal dynamics of aerobic anoxygenic phototrophs in freshwater lake Vlkov. *Folia Microbiologica* 64: 705–710.

Kolber Z.S., Plumley F.G., Lang A.S., Beatty J.T., Blankenship R.E., VanDover C.L., Vetriani C., Koblizek M., Rathgeber C. & Falkowski P.G. 2001. Contribution of aerobic photoheterotrophic bacteria to the carbon cycle in the ocean. *Science* 292: 2492–2495.

Kopejtka K., Tomasch J., Zeng Y., Selyanin V., Dachev M., Piwosz K., Tichý M., Bína D., Gardian Z., Bunk B., Brinkmann H., Geffers R., Sommaruga R. & Koblížek M. 2020. Simultaneous Presence of Bacteriochlorophyll and Xanthorhodopsin Genes in a Freshwater Bacterium. *mSystems* 5.

Kopejtka K., Zeng Y., Kaftan D., Selyanin V., Gardian Z., Tomasch J., Sommaruga R. & Koblížek M. 2021. Characterization of the Aerobic Anoxygenic Phototrophic Bacterium Sphingomonas sp. AAP5. *Microorganisms 2021, Vol. 9, Page 768* 9: 768.

Krueger B.P., Scholes G.D., Jimenez R. & Fleming G.R. 1998. Electronic excitation transfer from carotenoid to bacteriochlorophyll in the purple bacterium Rhodopseudomonas acidophila. *Journal of Physical Chemistry B* 102: 2284–2292.

Lennarz W. & Lane M. 2013. *Encyclopedia of biological chemistry*. Academic Press.

Lind L. 2021. Fabry-Perot-based hyperspectral reflectance imaging of asteroids.

Lloyd K.G., Steen A.D., Ladau J., Yin J. & Crosby L. 2018. Phylogenetically Novel Uncultured Microbial Cells Dominate Earth Microbiomes. *mSystems* 3.

Molisch H. 1907. Die Purpurbakterien : nach neuen Untersuchungen; eine Mikrobiologische Studie. *G. Fischer, Jena. p. 1–95*.

Müller D.J., Schabert F.A., Büldt G. & Engel A. 1995. Imaging purple membranes in aqueous solutions at sub-nanometer resolution by atomic force microscopy. *Biophysical Journal* 68: 1681–1686.

Nissinen R.M., Männistö M.K. & Elsas J.D. van. 2012. Endophytic bacterial communities in three arctic plants from low arctic fell tundra are cold-adapted and host-plant specific. *FEMS Microbiology Ecology* 82: 510–522.

O'Callahan B.T., Park K.D., Novikova I. v., Jian T., Chen C.L., Muller E.A., El-Khoury P.Z., Raschke M.B. & Lea A.S. 2020. In Liquid Infrared Scattering Scanning Near-Field Optical Microscopy for Chemical and Biological Nanoimaging. *Nano Letters* 20: 4497–4504.

Olsen J.D., Sockalingum G.D., Robert B. & Hunter C.N. 1994. Modification of a hydrogen bond to a bacteriochlorophyll a molecule in the light-harvesting 1 antenna of Rhodobacter sphaeroides. *Proceedings of the National Academy of Sciences of the United States of America* 91: 7124–7128.

Pfitzner E., Seki H., Schlesinger R., Ataka K. & Heberle J. 2018. Disc Antenna Enhanced Infrared Spectroscopy: From Self-Assembled Monolayers to Membrane Proteins. *ACS Sensors* 3: 984–991.

Pierson B.K. & Howard H.M. 1972. Detection of Bacteriochlorophyll-containing Micro-organisms by Infrared Fluorescence Photomicrography. *Microbiology* 73: 359–363.

Qian P., Addlesee H.A., Ruban A. v., Wang P., Bullough P.A. & Hunter C.N. 2003. A Reaction Center-Light-harvesting 1 Complex (RC-LH1) from a Rhodospirillum rubrum Mutant with Altered Esterifying Pigments: Characterization by Optical Spectroscopy and Cryo-electron Microscopy. *Journal of Biological Chemistry* 278: 23678–23685.

Ritz T., Damjanovic A. & Schulten K. 2002. The Quantum Physics of Photosynthesis. *Biophysics Special ChemPhysChem* 3: 243–248.

Ruban A. v. & Johnson M.P. 2015. Visualizing the dynamic structure of the plant photosynthetic membrane. *Nature Plants 2015 1:11* 1: 1–9.

Salka I., Srivastava A., Allgaier M. & Grossart H.P. 2014. The Draft Genome Sequence of Sphingomonas sp. Strain FukuSWIS1, Obtained from Acidic Lake Grosse Fuchskuhle, Indicates Photoheterotrophy and a Potential for Humic Matter Degradation. *Genome Announcements* 2.

Sato Takabe Y., Hamasaki K. & Suzuki K. 2012. Photosynthetic characteristics of marine aerobic anoxygenic phototrophic bacteria Roseobacter and Erythrobacter strains. *Archives of Microbiology* 194: 331–341.

Sato-Takabe Y., Hamasaki K. & Suzuki K. 2014. Photosynthetic Competence of the Marine Aerobic Anoxygenic Phototrophic Bacterium Roseobacter sp. under Organic Substrate Limitation. *Microbes and Environments* 29: 100–103.

Scheuring S., Boudier T. & Sturgis J.N. 2007. From high-resolution AFM topographs to atomic models of supramolecular assemblies. *Journal of Structural Biology* 159: 268–276.

Scheuring S. & Sturgis J.N. 2009. Atomic force microscopy of the bacterial photosynthetic apparatus: Plain pictures of an elaborate machinery. *Photosynthesis Research* 102: 197–211.

Scheuring S., Sturgis J.N., Prima V., Bernadac A., Lévy D. & Rigaud J.L. 2004. Watching the photosynthetic apparatus in native membranes. *Proceedings of the National Academy of Sciences of the United States of America* 101: 11293–11297.

Schwalbach M.S. & Fuhrman J.A. 2005. Wide-ranging abundances of aerobic anoxygenic phototrophic bacteria in the world ocean revealed by epifluorescence microscopy and quantitative PCR. *Limnology and Oceanography* 50: 620–628.

Sebban P. & Moya I. 1983. Fluorescence lifetime spectra of in vivo bacteriochlorophyll at room temperature. *Biochimica et Biophysica Acta (BBA) - Bioenergetics* 722: 436–442.

Selyanin V., Hauruseu D. & Koblížek M. 2015. The variability of light-harvesting complexes in aerobic anoxygenic phototrophs. *Photosynthesis Research* 128: 35–43.

Shiba T. & Simidu U. 1982. Erythrobacter longus gen. nov., sp. nov., an aerobic bacterium which contains bacteriochlorophyll a. *International Journal of Systematic Bacteriology* 32: 211–217.

Shiba T., Simidu U. & Taga N. 1979. Distribution of Aerobic Bacteria Which Contain Bacteriochlorophyll a. *Applied and Environmental Microbiology* 38: 43–45.

Šlouf V., Fuciman M., Dulebo A., Kaftan D., Koblížek M., Frank H.A. & Polívka T. 2012. Carotenoid charge transfer states and their role in energy transfer processes in LH1-RC complexes from aerobic anoxygenic phototrophs. *The Journal of Physical chemistry. B* 117: 10987–10999.

Stiefel P., Zambelli T. & Vorholta J.A. 2013. Isolation of optically targeted single bacteria by application of fluidic force microscopy to aerobic anoxygenic phototrophs from the phyllosphere. *Applied and Environmental Microbiology* 79: 4895–4905.

Subczynski W.K., Markowska E., Gruszecki W.I. & Sielewiesiuk J. 1992. Effects of polar carotenoids on dimyristoylphosphatidylcholine membranes: a spin-label study. *Biochimica et Biophysica Acta (BBA) - Biomembranes* 1105: 97–108.

Tang K., Yang L.H., Chen Y.P., Tao Y., Feng F.Y. & Meng J.Y. 2021. Aerophototrophica crusticola gen. Nov., sp. nov., isolated from desert biocrusts. *International Journal of Systematic and Evolutionary Microbiology* 71: 004677.

Tang K., Zong R., Zhang F., Xiao N. & Jiao N. 2010. Characterization of the photosynthetic apparatus and proteome of roseobacter denitrificans. *Current Microbiology* 60: 124–133.

Trudel E., Gallant J., Mons S., Mioskowski C., Lebeau L., Jeuris K., Foubert P., Schryver F. de & Salesse C. 2001. Design of functionalized lipids and evidence for their binding to photosystem II core complex by oxygen evolution measurements, atomic force microscopy, and scanning near-field optical microscopy. *Biophysical journal* 81: 563–571.

Unsay J.D., Cosentino K. & García-Sáez A.J. 2015. Atomic Force Microscopy Imaging and Force Spectroscopy of Supported Lipid Bilayers. *Journal of Visualized Experiments : JoVE* 2015: 1–9.

Worcester D.L., Kim H.S., Miller R.G. & Bryant P.J. 1990. Imaging bacteriorhodopsin lattices in purple membranes with atomic force microscopy. *Journal of Vacuum Science & Technology A: Vacuum, Surfaces, and Films* 8: 403.

Yabuuchi E., Kosako Y., Fujiwara N., Naka T., Matsunaga I., Ogura H. & Kobayashi K. 2002. Emendation of the genus Sphingomonas Yabuuchi et al. 1990 and junior objective synonymy of the species of three genera, Sphingobium, Novosphingobium and Sphingopyxis, in conjunction with Blastomonas ursincola. *International Journal of Systematic and Evolutionary Microbiology* 52: 1485–1496.

Yabuuchi E., Yano I., Oyaizu H., Hashimoto Y., Ezaki T. & Yamamoto H. 1990. Proposals of Sphingomonas paucimobilis gen. nov. and comb. nov., Sphingomonas parapaucimobilis sp. nov., Sphingomonas yanoikuyae sp. nov., Sphingomonas adhaesiva sp. nov., Sphingomonas capsulata comb, nov., and Two Genospecies of the Genus Sphingomonas. *Microbiology and Immunology* 34: 99–119.

Yurkov V. v. & Beatty J.T. 1998. Aerobic Anoxygenic Phototrophic Bacteria. *Microbiology and Molecular Biology Reviews* 62: 695.

Yurkov V. & Csotonyi J.T. 2009. New Light on Aerobic Anoxygenic Phototrophs. : 31–55.

Yurkov V., Gad'on N. & Drews G. 1993. The major part of polar carotenoids of the aerobic bacteria Roseococcus thiosulfatophilus RB3 and Erythromicrobium ramosum E5 is not bound to the bacteriochlorophyll a-complexes of the photosynthetic apparatus. *Archives of Microbiology 1993 160:5* 160: 372–376.

Yurkov V. & Hughes E. 2017. Aerobic anoxygenic phototrophs: Four decades of mystery. *Modern Topics in the Phototrophic Prokaryotes: Environmental and Applied Aspects*: 193–214.

Zeng Y., Feng F., Medová H., Dean J. & Koblížek M. 2014. Functional type 2 photosynthetic reaction centers found in the rare bacterial phylum Gemmatimonadetes. *Proceedings of the National Academy of Sciences of the United States of America* 111: 7795–7800.

Zervas A., Zeng Y., Madsen A.M., Hansen L.H. & Martinez-Romero E. 2019. Genomics of Aerobic Photoheterotrophs in Wheat Phyllosphere Reveals Divergent Evolutionary Patterns of Photosynthetic Genes in Methylobacterium spp. *Genome Biology and Evolution* 11: 2895–2908.

Zhang D.C., Busse H.J., Liu H.C., Zhou Y.G., Schinner F. & Margesin R. 2011. Sphingomonas glacialis sp. nov., a psychrophilic bacterium isolated from alpine glacier cryoconite. *International Journal of Systematic and Evolutionary Microbiology* 61: 587–591.